The Journal of Immunology

RESEARCH ARTICLE | DECEMBER 15 2017

# CD27-Mediated Regulatory T Cell Depletion and Effector T Cell Costimulation Both Contribute to Antitumor Efficacy

Anna Wasiuk; ... et. al

*J Immunol* (2017) 199 (12): 4110–4123.
https://doi.org/10.4049/jimmunol.1700606

# CD27-Mediated Regulatory T Cell Depletion and Effector T Cell Costimulation Both Contribute to Antitumor Efficacy

**Anna Wasiuk,* James Testa,* Jeff Weidlick,* Crystal Sisson,* Laura Vitale,* Jenifer Widger,* Andrea Crocker,* Lawrence J. Thomas,† Joel Goldstein,* Henry C. Marsh,† Tibor Keler,* and Li-Zhen He***

**CD27, a member of the TNFR superfamily, is constitutively expressed in most T cells and plays crucial roles in T cell effector functions. The costimulation and antitumor activity of CD27 agonistic Abs have been well documented in mouse models. Clinical testing of a human IgG1 anti-CD27 Ab, varlilumab (clone 1F5), is ongoing in cancer patients. In this study, we set out to further understand CD27 as an immunomodulatory target and to address the mechanism of antitumor efficacy using different IgG isotypes of 1F5 in human *CD27*-transgenic mice. 1F5mIgG1, the only isotype engaging inhibitory FcγRIIB expressed in B cells, elicited the most potent and broad immune response, but terminal differentiation, exhaustion, and apoptosis in the activated effector T cells were inevitable. Accordingly, this isotype was the most effective in eradicating BCL1 lymphoma but had limited efficacy in s.c. tumors. Conversely, 1F5mIgG2a, which interacts with cells expressing activating FcγRs, led to moderate immune activation, as well as to prominent reduction in the number and suppressive activity of regulatory T cells. These combined mechanisms imparted potent antitumor activity to 1F5mIgG2a, particularly against the s.c. tumors. 1F5hIgG1, varlilumab, showed balanced agonistic activity that was prominent at lower doses and depleting activity that was greater at higher doses. 1F5hIgG1 had good antitumor activity in all tumor models tested. Thus, both agonist and depleting properties contribute to the antitumor efficacy of CD27-targeted immunotherapy, and modulation of these activities in patients may be achieved by varying the dose and regimen. *The Journal of Immunology*, 2017, 199: 4110–4123.**

Blockade of checkpoint inhibitors, such as CTLA-4 and programmed cell death protein 1 (PD-1)/programmed cell death ligand 1, with Abs has shown remarkable therapeutic benefits in a variety of cancers (1–5). Triggering costimulatory signals via TNFR superfamily (TNFRSF) members, such as CD27, OX40 (CD134), 4-1BB (CD137), and glucocorticoid-induced TNFR-related protein (GITR), on T cells is another promising approach in the development of cancer immunotherapy (6, 7). The concept of "releasing the brakes and pressing the gas pedal" is a simplified description of how immunomodulation works but underscores the rationale for synergy by targeting both coinhibitory molecules with antagonists and costimulatory molecules with agonists. However, the mechanism of action (MOA) for immunomodulatory Abs is not well understood, and maximal harnessing of immunity through T cell–costimulatory receptors to achieve prominent and long-lasting effector function is complicated by their varying roles in different T cell populations and their differentiation state. For example, depletion of regulatory T cells ($T_{reg}$) has been reported, at least in mouse models, to be a common indispensable MOA for the antitumor efficacy of Abs that target costimulatory OX40 and GITR or coinhibitory CTLA4 (8–10). Our interest has been focused on understanding CD27 as a target for Ab-mediated immunomodulatory therapy.

CD27, unlike other members of the TNFRSF, is constitutively expressed on most T cells, including naive and effector CD4 and CD8 T cells. CD27 signaling is controlled by its ligand, CD70, the expression of which is transient upon activation of dendritic cells (DCs), B cells, and T cells, and is tightly regulated (11–13). CD70–CD27 interaction provides a potent second signal for CD4 T cell–dependent and -independent CD8 T cell priming, effector differentiation, and memory development in virus clearance or tumor rejection (14–25). Human CD27 or CD70 deficiency due to genetic mutations resulted in persistent symptomatic EBV infection and EBV-associated lymphoproliferative disorders, including lethal lymphoma (26–30). In contrast, triggering CD27 persistently, such as by constitutively expressing CD70 in transgenic mouse models, resulted in a progressive and ultimately lethal deficiency in T cells, NK cells, and B cells due to direct exhaustion and activation-induced cell death (AICD) or IFN-γ–mediated indirect depletion (31–34). Prolonged CD70 expression on T and B cells during chronic virus infection also led to inflammatory cytokine-mediated destruction of splenic architecture, immunodeficiency with impaired CD8 T cell responses, and virus-specific neutralizing Ab responses (34–36). Therefore, CD27 signaling either improved the function of or

*Celldex Therapeutics, Inc., Hampton, NJ 08827; and †Celldex Therapeutics, Inc., Needham, MA 02494

ORCIDs: 0000-0003-4691-7829 (J. Widger); 0000-0002-5343-406X (L.J.T.); 0000-0001-5637-6013 (H.C.M.); 0000-0001-8206-761X (L.-Z.H.).

Received for publication April 27, 2017. Accepted for publication October 7, 2017.

This work was supported by Celldex Therapeutics, Inc.

Address correspondence and reprint requests to Dr. Li-Zhen He, Celldex Therapeutics, Inc., 53 Frontage Road, Suite 220, Hampton, NJ 08827. E-mail address: lhe@celldex.com

The online version of this article contains supplemental material.

Abbreviations used in this article: aCasp3, active caspase 3; ADCC, Ab-dependent cell-mediated cytotoxicity; ADCP, Ab-dependent cell-mediated phagocytosis; AICD, activation-induced cell death; B6, C57BL/6; DC, dendritic cell; Eomes, eomesodermin; GITR, glucocorticoid-induced TNFR-related protein; GzmB, granzyme B; h*CD27*-Tg, human *CD27*–transgenic; hG1, human IgG1; KLRG1, killer cell lectin-like receptor subfamily G member 1; Lag-3, lymphocyte activation gene 3; mG1, mouse IgG1; mIgG, mouse IgG; mG2a, mouse IgG2a; MOA, mechanism of action; NKG2D, NK group 2 member D; PD-1, programmed cell death protein 1; pLN, peripheral lymph node; SLEC, short-lived effector cell; $T_{cm}$, central memory T cell; TdLN, tumor-draining lymph node; $T_{em}$, effector memory T cell; TIL, tumor-infiltrating lymphocyte; Tim-3, T cell Ig and mucin-domain containing-3; TNFRSF, TNFR superfamily; $T_{reg}$, regulatory T cell.

enhanced the exhaustion and death of effector T cells, depending on the strength, duration, and timing of the agonistic stimulation (16, 17, 35, 37). Additionally, slower tumor growth in *CD27*$^{-/-}$ mice due to diminished $T_{reg}$ numbers was reported, supporting the role of CD70–CD27 interaction in the generation and survival of $T_{reg}$ (38, 39).

Targeting CD27 to enhance CD8 T cell responses and antitumor activity was originally demonstrated with agonistic anti-mouse CD27 Abs and soluble CD70 (40–44). We previously reported the generation and characterization of a human IgG1 (hG1) anti-human CD27 Ab, varlilumab (clone 1F5) (45). Using a human CD27-transgenic (h*CD27*-Tg) mouse model, the agonistic activity and T cell–mediated antitumor efficacy of varlilumab have been well documented (46). As generally true for agonistic Abs that target other TNFRSF members, cross-linking or engagement of FcγRs is essential for varlilumab to exert costimulatory activity and antitumor efficacy (46). A phase I clinical trial of varlilumab showed a favorable safety profile and promising signs of immunological and clinical responses in advanced treatment–refractory cancer patients (47). A phase II clinical trial of varlilumab in combination with anti–PD-1 nivolumab in multiple advanced cancers is ongoing (NCT02335918).

Previous studies have documented that Abs targeting TNFRSF, such as CD40, OX40, and GITR, result in costimulation or depletion of the target-expressing cells, depending on the FcγRs that are engaged by the Fc portion of the Abs (9, 10, 48, 49). In general, when the Abs are formatted as mouse IgG1 (mG1), they lack the activity of triggering effector cell functions, such as Ab-dependent cell-mediated cytotoxicity (ADCC) and Ab-dependent cell-mediated phagocytosis (ADCP), because they preferentially engage inhibitory FcγRIIB expressed on abundant B cells, which allows for efficient cross-linking and costimulation of the Abs. Conversely, the mouse IgG2a (mG2a) mainly interacts with activating FcγRI, FcγRIII, and FcγRIV expressed on NK, macrophages, and neutrophils and thus has potent effector cell function and the potential for depleting cells that express sufficient level of the targets. In this study, we generated mG1 and mG2a isotype variants of varlilumab to differentially drive interaction with inhibitory and activating FcγRs, which predictably promoted CD27-mediated agonism or depletion, respectively. We tested antitumor activity of the varlilumab variants (designated 1F5mG1 and 1F5mG2a) along with varlilumab (1F5hG1) in multiple syngeneic tumor models. Surprisingly, different isotype variants of 1F5 showed distinct antitumor efficacy in the tumor models tested. Although 1F5mG1 induced dramatic T cell proliferation and activation and controlled the growth of BCL1 lymphoma, the potent CD27 signaling resulted in terminal differentiation, exhaustion, and apoptosis of the activated T cells and, thus, limited memory generation. 1F5mG2a had more limited immune activation properties but depleted CD27$^{hi}$ cells, especially $T_{reg}$, which led to cure in some mice bearing E.G7, Colon26, and CT26 tumors. Interestingly, the residual $T_{reg}$ after 1F5mG2a treatment had poor suppressive activity, unlike the residual $T_{reg}$ following PC.61 treatment, a commonly used CD25 Ab for $T_{reg}$ depletion. This was associated with better antitumor activity of 1F5mG2a relative to PC.61. 1F5hG1 possessed both agonistic and depleting activities to a moderate extent, leading to potent antitumor efficacy in a broader tumor spectrum. Analyses of immune correlates in the tumor microenvironment and tumor-draining lymph nodes (TdLNs) further elucidated the dynamics of the antitumor immune responses and the development of protective memory upon targeting CD27 with agonistic or depleting Abs and underscore the advantages of combining these dual mechanisms.

## Materials and Methods

### *Generation of mouse IgG variants of anti-human CD27 Ab 1F5*

Anti-human CD27 1F5hG1 was generated and characterized as described previously (45). 1F5 H and L chain variable regions were cloned to substitute the counterparts of irrelevant mG1 and mG2a in an expression vector. A D265A mutation was introduced into the mouse γ 1 sequence by site-directed mutagenesis (Stratagene). The replacement of variable regions and the D265A mutation were validated by DNA sequencing. The resultant 1F5mG1, 1F5mG2a, and 1F5mG1$_{D265A}$ were produced by standard transfectoma and chromatography-purification technologies. The retention of human CD27 binding capacity of 1F5 variants was confirmed by functional ELISA and flow cytometry. The distinct binding affinity and kinetics of 1F5 variants to mouse FcγRs (R&D Systems) were examined by surface plasmon resonance analysis using a Biacore 2000 SPR instrument (Biacore AB, Uppsala, Sweden). The endotoxin level for all Abs used in functional assays or in vivo studies was <1.0 EU/mg, as measured by the Gel Clot LAL method (Lonza).

### *In vivo administration*

The h*CD27*-Tg mice were genetically engineered and backcrossed onto the C57BL/6 (B6) and BALB/c strains (46). Wild-type breeding mates were purchased from Taconic Biosciences. All mice were housed under specific pathogen–free conditions in our animal facilities and used in accordance with the guidelines established by the Institutional Animal Care and Use Committee at Celldex Therapeutics. All experiments were performed using the B6 heterozygous h*CD27*-Tg mouse strain, with the exception of studies using the syngeneic tumor models BCL1, CT26, and Colon26, which were performed in BALB/c h*CD27*-Tg heterozygous mice. Equal numbers of male or female mice were allocated to each group in all studies. All mice were 6–12 wk of age when studies were initiated, and the age span within each study was 2 wk. The B6 heterozygous h*CD27*-Tg strain is CD45.1 and CD45.2 double positive, and these congenic markers were used in E.G7 tumor–infiltration analyses. h*CD27*-Tg mice were injected i.p. with 10–250 μg of 1F5 variants, with or without 5 mg of OVA (Sigma-Aldrich). CD25 Ab PC.61 (Bio X Cell) was injected i.p. in the range of 200–400 μg. Mouse IgG (mIgG; Bio X Cell), 1F5mG1$_{D265A}$, or irrelevant hG1 alternately served as background controls. Spleen and peripheral lymph nodes (pLNs) were collected for SIINFEKL-tetramer staining, IFN-γ–ELISPOT assay, and cell surface and intracellular staining.

### *Tumor challenge studies*

The antitumor efficacy of 1F5 variants was evaluated in multiple mouse syngeneic tumor models. BCL1, a B cell lymphoma (kindly provided by Dr. M. Glennie, University of Southampton), was maintained and expanded in vivo in female BALB/c mice, and $5 \times 10^6$ cells from an in vivo spleen passage were inoculated i.v. into h*CD27*-Tg mice for tumor-challenge studies. E.G7 (American Type Culture Collection), an EL4-derived thymoma, was grown in RPMI 1640/10% FBS/penicillin/streptomycin/0.4 mg/ml G418, and $0.5 \times 10^6$ cells were used for s.c. inoculation. Colon carcinomas CT26 (American Type Culture Collection) and Colon26 (National Cancer Institute) were cultured in RPMI 1640/10% FBS/penicillin/streptomycin, and $1.5 \times 10^4$ CT26 cells or $0.5 \times 10^6$ Colon26 cells were used for s.c. inoculation. B16-MUC1, a MUC1 p40 peptide–expressing derivative of B16 melanoma (kindly provided by Oncothyreon, selected to use because of its feature of slower growth than the parental B16 tumor), was cultured in DMEM/10% FBS/penicillin/streptomycin/0.3 mg/ml G418, and $0.2 \times 10^6$ cells were used for s.c. inoculation. These models all tested negative for CD70 and CD27 expression by flow cytometry, and the levels of soluble CD27 in blood were not significantly different from baseline at the time around treatment initiation (data not shown). Tumor-inoculated mice were treated i.p. with 1F5 variants at a dose of 100 or 200 μg, once or repeatedly, as indicated in the figure legends. Control groups consisted of h*CD27*-Tg mice that were injected with mIgG or saline or were left untreated. PC.61 alone or in combination with 1F5mG2a was administered i.p. 7 d prior to E.G7 tumor inoculation for the comparison of these two Abs. Mice were checked daily for general health status. Tumors were measured twice a week using calipers, and volumes were calculated using a modified ellipsoid formula [$V = 1/2$ (length $\times$ width$^2$)]. Mice were euthanized upon reaching predefined end points approved by the Institutional Animal Care and Use Committee. Secondary tumor challenge was performed in mice free of tumors and ≥60 d post–primary tumor inoculation, and a group of five or six naive mice was included to observe tumor growth. No further treatment was administered upon rechallenge.

### *Surface, tetramer, and intracellular staining for flow cytometry*

Single-cell suspensions from spleen, lymph nodes, and tumor samples were stained first with blue-fluorescent reactive dye (Live/Dead Fixable Dead Cell Stain Kit; Invitrogen) to exclude dead cells from analysis, then for surface markers, and subsequently for intracellular or intranuclear molecules, following fixation and permeabilization with the Cytofix/Cytoperm or Foxp3 Buffer Set (BD Biosciences and eBioscience). Fluorescence dye–conjugated Abs for cell surface CD3 (clone 145-2C11), CD4 (clone GK1.5), CD8 (clone 53-6.7), CD25 (PC61.5), CD44 (clone IM7), CD62L (clone MEL-14), CD127 (clone A7R34), killer cell lectin-like receptor subfamily G member 1 (KLRG1; clone 2F1), PD-1 (clone J43), T cell Ig and mucin-domain containing-3 (Tim-3; clone RMT3-23), lymphocyte activation gene 3 (Lag-3; clone C9B7W), Fas (CD95; clone Jo2), human CD27 (clone MT271, noncompetitive with 1F5 binding), NK1.1 (clone PK136), CD11c (clone HL3), CD40 (clone 3/23), CD86 (clone GL1), CD45.1 (clone A20), CD45.2 (clone 104), CD19 (clone 1D3), NK group 2 member D (NKG2D; clone CX5), MHC class II I-A/I-E (clone M5/114); for intracellular IFN-γ (clone XMG1.2), TNF-α (clone MP6-XT22), IL-2 (clone JES6-5H4), granzyme B (GzmB; clone GB11), active caspase 3 (aCasp3; clone C92-605), and Bcl-2 (clone 3F11); and for intranuclear Foxp3 (clone MF23), eomesodermin (Eomes; Dan11mag), and Ki-67 (clone SolA15) were purchased from BD Biosciences, eBioscience, BioLegend, or Invitrogen. The gating strategy always included pregating on live cells (blue dye negative) and then gating on $CD11c^{+}MHCII^{hi}$ for DCs, $NK1.1^{+}$ for NK cells, or CD3, CD4, or CD8 for T cells. $T_{reg}$ were defined as $CD4^{+}Foxp3^{+}$ or $CD4^{+}CD25^{+}$, as indicated in the figure legends. CD4 Th cells were defined as $CD4^{+}Foxp3^{-}$, except for being used as responders in the $T_{reg}$-suppression assay ($CD4^{+}CD25^{-}$). Because $T_{reg}$ account for only ~10% of total CD4 T cells (50), CD4 T cells (i.e., total $CD4^{+}$ cells or $CD3^{+}CD8^{-}$ cells) were alternatively used to represent CD4 Th cells. CD8 T cells were $CD8^{+}$ cells or $CD3^{+}CD4^{-}$ cells. Tumor-infiltrating leukocytes (TILs) were identified as $CD45.1^{+}$ cells, and tumor cells were identified as $CD45.1^{-}$. Events were acquired using a FACSCanto II flow cytometer and analyzed using FCS Express V4 software.

For cytokine staining, $1 \times 10^{6}$ cells were incubated in the presence or absence of 2 μg/ml SIINFEKL peptide or CD3 Ab (clone 145-2C11), plus CD28 Ab (clone 37.51) for 5 h. Brefeldin A (10 μg/ml; Sigma-Aldrich) was added for the last 4 h. Tetramer staining was performed using the iTAg H-2 Kb OVA (SIINFEKL) tetramer (MBL) at room temperature for 30 min following live/dead and surface staining. CD8 Ab (clone KT15; MBL) was used to minimize nonspecific tetramer staining.

### *$T_{reg}$ suppressive activity assay*

h*CD27*-Tg mice were injected i.p. with 100 or 200 μg of 1F5 variants or with 200 μg of PC.61 on day 0. Spleens were collected on day 7, and $T_{reg}$ were isolated using the MACS $CD4^{+}CD25^{+}$ Regulatory T Cell Isolation Kit, mouse (Miltenyi Biotec). Responder CD4 Th cells ($CD4^{+}CD25^{-}$) and CD8 T cells were isolated from naive mouse splenocytes using the above $T_{reg}$ isolation kit and CD8α MicroBeads in conjunction with MACS columns, respectively. CD4 Th cells and CD8 T cells were labeled with CFSE (Invitrogen), mixed with $T_{reg}$ at a 1:1 ratio, and cultured in triplicate in a 96-well U-bottom tissue culture plate predry coated with CD3 Ab for CD8 responders (0.05 micrograms per well) and CD4 Th responders (0.2 micrograms per well). CD28 Ab (2 μg/ml) was added to the $T_{reg}$ and



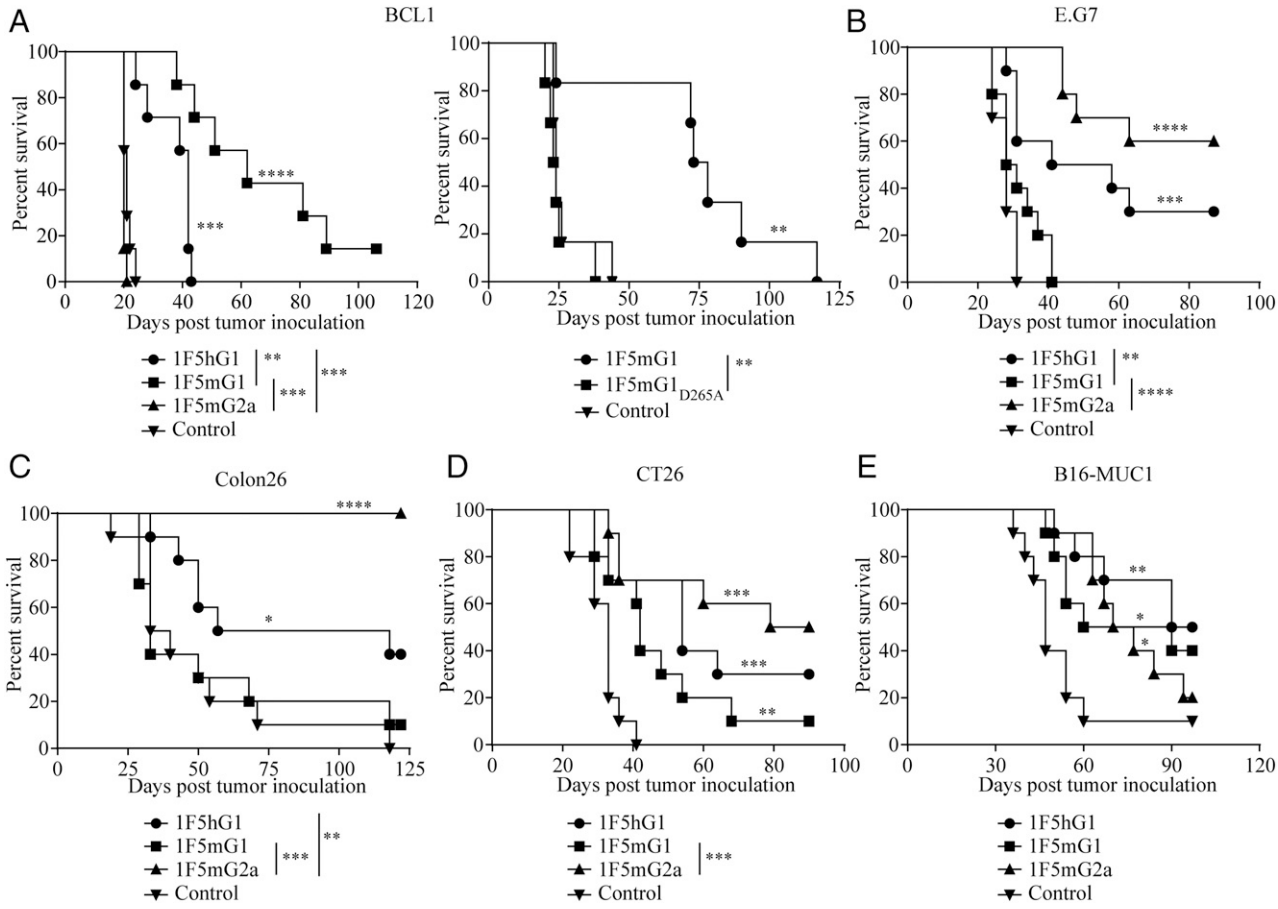


**FIGURE 1.** 1F5 variants elicit model-dependent antitumor efficacy. (**A**) Groups of seven (left panel) or six (right panel) h*CD27*-Tg BALB/c mice were inoculated i.v. with $5 \times 10^{6}$ BCL1 cells on day 0 and treated with 200 μg of 1F5 variants or saline on day 5. (**B**) Groups of 10 h*CD27*-Tg B6 mice were inoculated s.c. with $0.5 \times 10^{6}$ E.G7 cells on day 0 and treated with 200 μg of 1F5 variants or control IgG on days 3, 10, and 17. (**C**) Groups of 10 h*CD27*-Tg BALB/c mice were inoculated s.c. with $0.5 \times 10^{6}$ Colon26 cells on day 0 and treated with 200 μg of 1F5 variants or control IgG on days 7, 14, 21, and 28. (**D**) Groups of 10 h*CD27*-Tg BALB/c mice were inoculated s.c. with $1.5 \times 10^{4}$ CT26 cells on day 0 and treated with 200 μg of 1F5 variants or control IgG on days 3, 5, 7, 9, and 11. (**E**) Groups of 10 h*CD27*-Tg B6 mice were inoculated s.c. with $0.2 \times 10^{6}$ B16-MUC1 cells on day 0 and treated with 100 μg of 1F5 variants on days 5, 8, 12, 15, 19, and 22 or left untreated. Tumor size was measured twice a week, and mice were monitored daily for survival. Data are representative of two or three independent studies for each tumor model. Vertical lines indicate statistical significance between groups specified. $*p < 0.05$, $**p < 0.01$, $***p < 0.001$, $****p < 0.0001$ versus control IgG, saline, or untreated group.

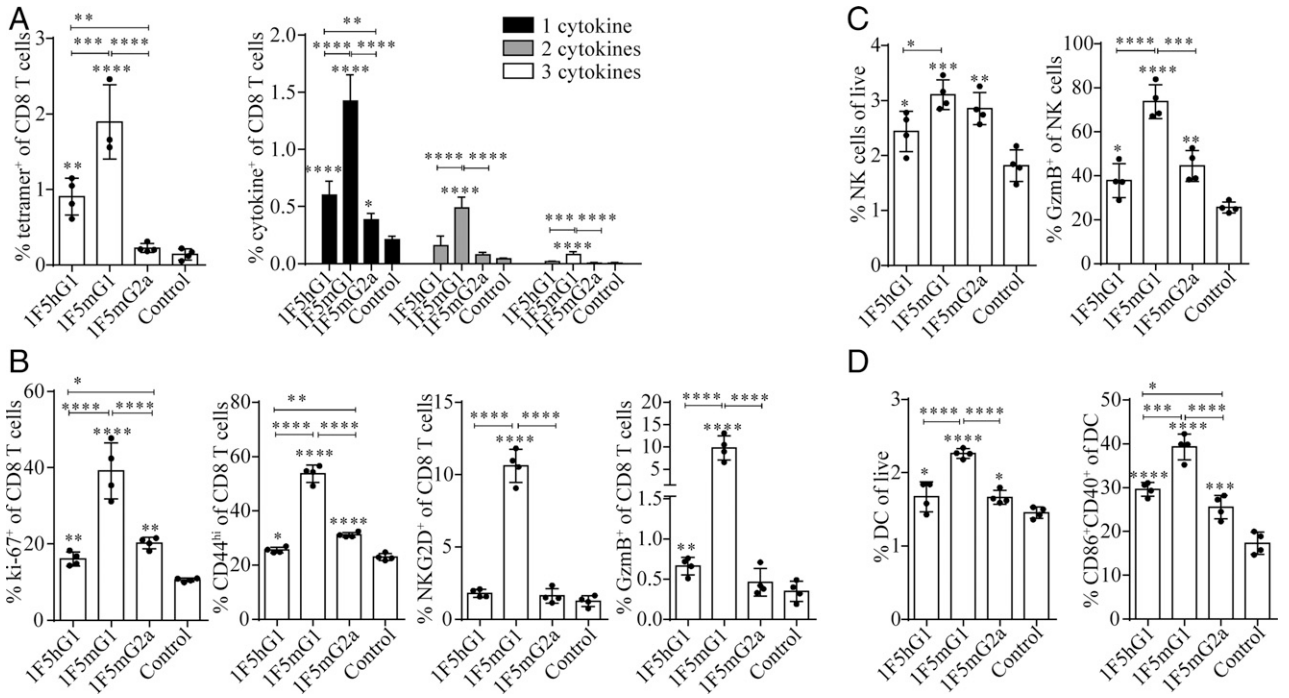


**FIGURE 2.** Potent agonistic CD27 signaling drives a robust and broad immune response. (**A**) h*CD27*-Tg B6 mice were injected i.p. with 5 mg of OVA and 50 μg of 1F5 variants on day 0. Ag-specific CD8 T cell responses were assessed in the spleen 7 d later. Shown are SIINFEKL-tetramer$^+$ cells within gated CD8 T cells, as well as intracellular IFN-γ, TNF-α, and IL-2 single-, double-, or triple-positive CD8 T cells after ex vivo stimulation with SIINFEKL peptide and CD28 Ab. (**B**) h*CD27*-Tg B6 mice were injected i.p. with 200 μg of 1F5 variants on day 0. Overall CD8 T cell responses were assessed in the spleen 7 d later. Surface CD44 and NKG2D, intracellular GzmB, and intranuclear Ki-67 staining within gated CD8 T cells without ex vivo stimulation are shown. (**C** and **D**) NK and DC populations and their activation were assessed in the same splenocytes as in (B). Cells were stained with NK1.1 for NK cells and dual stained with CD11c and MHC class II for DCs. Intracellular GzmB in gated NK cells and surface CD86 and CD40 in gated DCs are shown. Data are representative of four independent experiments ($n$ = 3 or 4 mice per group). Horizontal lines above the bars indicate statistical significance between the groups specified. *$p < 0.05$, **$p < 0.01$, ***$p < 0.001$, ****$p < 0.0001$ versus control IgG.

CD8 T cell cocultures. All of the cocultures were incubated at 37°C for 3 d, and brefeldin A (10 μg/ml) was added for the last 4 h. Cells were then stained for surface CD4 and CD8 and intracellular IFN-γ, as described above. Baseline $T_{reg}$-suppressive activity was calculated as the difference in proliferation (CFSE dilution) and activation (IFN-γ$^+$ percentage) of CD4 Th and CD8 T cells between wells in the absence and presence of $T_{reg}$ isolated from 1F5mG1$_{D265A}$- or mIgG-treated control mice.

### *TIL and TdLN analysis*

hCD27-Tg BALB/c mice received $3.0 \times 10^6$ BCL1 cells i.v. on day 0 and 200 μg of 1F5 variants i.p. on day 5. Spleens were collected on day 12 and processed into single-cell suspensions by manually grinding using the frosted ends of microscope slides. Cell staining and flow cytometry analysis were performed as mentioned above.

h*CD27*-Tg B6 mice received $1.0 \times 10^6$ E.G7 cells s.c. on the right flank on day 0 and 200 μg of 1F5 variants i.p. on day −7 or day 4. Tumor and TdLNs were collected on days 7–10 or days 18–20. Tumors were processed into single-cell suspensions by manually mincing and then enzymatically digesting with Liberase TM and DNase I (48 μg/ml and 250 U/ml, respectively; Roche) in RPMI 1640 for 1 h at 37°C while rotating gently. GentleMACS C tubes and a gentleMACS dissociator (Miltenyi Biotec) were used to homogenize the tissue at the beginning, middle, and end of the incubation period. Digestion was quenched by adding RPMI 1640/10% FBS, and cells were filtered through 70-μm nylon strainers (Corning Life Sciences). Cell staining and flow cytometry analysis were performed as previously mentioned.

### *Statistical analysis*

GraphPad Prism 6 software was used for statistical analysis. Data are expressed as mean and SD. Data shown are representative of two to four repeated studies. The Student $t$ test and one-way and two-way ANOVA were used for comparisons between two or multiple groups. The Mantel–Cox test was used for survival curve comparison. The level of statistical significance is indicated as follows: *$p < 0.05$, **$p < 0.01$, ***$p < 0.001$, ****$p < 0.0001$.

## Results

### *Targeting CD27 with different isotypes of 1F5 Ab elicits model-dependent antitumor efficacy*

To study the mechanisms involved in the antitumor activities of varlilumab in h*CD27*-Tg mice, we generated mG1 and mG2a isotype variants of 1F5 to engage distinct FcγRs that would intentionally promote agonistic or depleting activities of the Ab, respectively. We first confirmed that altering the isotype of 1F5 did not affect its binding to soluble or cell surface human CD27 (data not shown, Supplemental Fig. 1A) and that the mouse FcγR binding profile of the 1F5 variants was consistent with expectations (48, 51). As expected, the introduction of a D265A mutation completely abrogated all FcγR binding; 1F5mG1 bound to FcγRIIB and FcγRIII, 1F5mG2a bound to FcγRI, FcγRIII, and FcγRIV, and 1F5hG1 preferentially bound to FcγRI and FcγRIV with relatively lower affinity compared with 1F5mG2a (Supplemental Fig. 1B).

We tested the antitumor activity of 1F5 variants in five syngeneic tumor models using the B6 or BALB/c strain of h*CD27*-Tg mice. We observed different levels of antitumor efficacy depending on the tumor model and isotype of 1F5. In the i.v. inoculated BCL1 lymphoma model that primarily grows in the spleen, treatment with 1F5mG1 was most effective, whereas 1F5mG2a was completely ineffective. 1F5hG1 also significantly extended survival compared with controls but not as effectively as 1F5mG1. However, 1F5mG1$_{D265A}$, lacking the ability to bind FcγRs, lost the antitumor efficacy (Fig. 1A). In the E.G7 and Colon26 models, tumor regression and long-term survival were achieved very effectively with 1F5mG2a, whereas the effect of 1F5mG1 was poor in these models. As in the BCL1 model, 1F5hG1 had intermediate

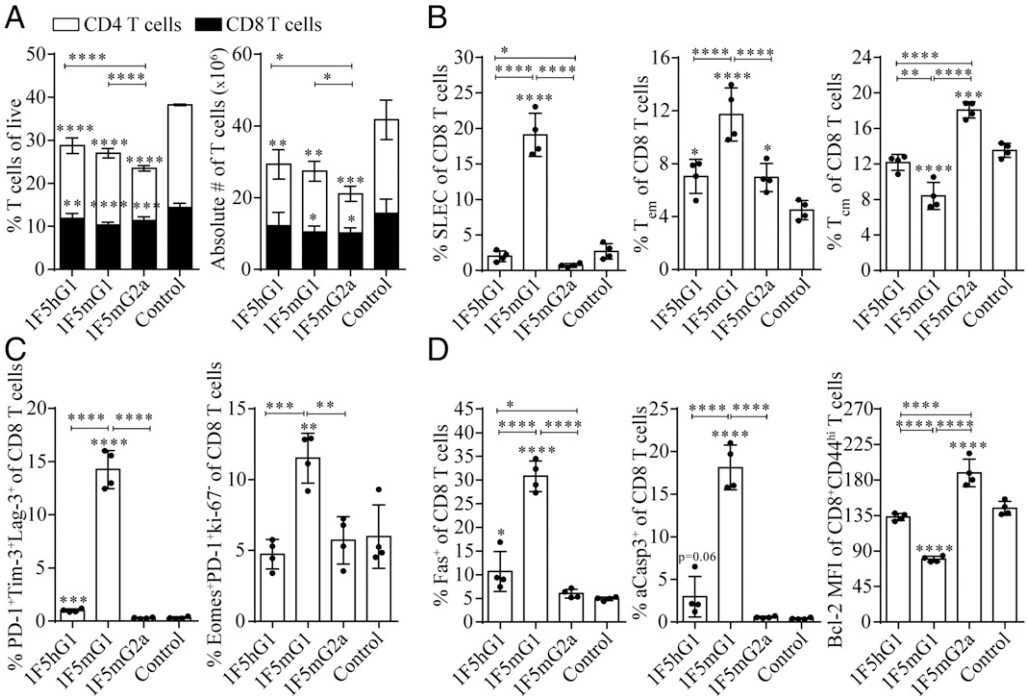


**FIGURE 3.** CD27 agonism induces terminal differentiation, exhaustion, and apoptosis of CD8 T cells. h*CD27*-Tg B6 mice were injected i.p. with 200 μg of 1F5 variants on day 0, and spleens were collected on day 7 for flow cytometric analysis. (**A**) Shown are the percentage of CD8 and CD4 T cells out of total live cells and their absolute numbers depicted in stacked bars. (**B**) Splenocytes were stained for the surface markers CD44, CD62L, CD127, and KLRG1. SLECs are defined as $CD127^-KLRG1^+CD44^{hi}CD62L^{lo}$, $T_{em}$ are defined as $CD127^+KLRG1^-CD44^{hi}CD62L^{lo}$, and $T_{cm}$ are defined as $CD127^+KLRG1^-CD44^{hi}CD62L^{hi}$; their percentages within gated CD8 T cells are shown. (**C**) Splenocytes were stained for the exhaustion markers PD-1, Tim-3, and Lag-3. Coexpression of these three markers within gated CD8 T cells are shown. Additionally, splenocytes were costained for surface PD-1, intranuclear Ki-67, and Eomes. (**D**) Splenocytes were stained for Fas and aCasp3, and their percentages within gated CD8 T cells are shown. Intranuclear Bcl-2 was stained in the same splenocytes, and the expression level (mean fluorescence intensity [MFI]) is depicted in gated $CD44^{hi}$ activated CD8 T cells. Data are representative of three independent experiments ($n$ = 3 or 4 mice per group), Horizontal lines indicate statistical significance between the groups specified. $^*p < 0.05$, $^{**}p < 0.01$, $^{***}p < 0.001$, $^{****}p < 0.0001$ versus control IgG.

activity (Fig. 1B, 1C). In two other models, CT26 and B16-MUC1, we observed less dramatic differences among the three isotypes of 1F5, all of which had at least partial efficacy (Fig. 1D, 1E). To study the mechanism of this model-dependent antitumor activity of 1F5mG1 versus 1F5mG2a, we characterized their impact on immune cell subsets and responses in spleen, pLNs, TILs, and TdLNs.

### *Potent agonistic CD27 signaling drives strong and broad immune responses but leads to AICD*

We first compared the immune responses enhanced by 1F5 variants in peripheral lymphoid organs. 1F5 variants were administered to h*CD27*-Tg mice receiving an OVA vaccine to quantify the enhancement of the T cell response as a readout of costimulation. As shown in Fig. 2A, 1F5mG1 elicited the highest costimulatory activity, followed by 1F5hG1; only a modest effect was observed with 1F5mG2a under these conditions. The increase in SIINFEKL-tetramer$^+$ staining among animals treated with the different isotypes of 1F5 was 13.5-, 6.5-, and 1.6-fold over control for 1F5mG1, 1F5hG1, and 1F5mG2a, respectively. This result was concurrent with the increase in SIINFEKL-specific IFN-γ–, TNF-α–, and IL-2–producing CD8 T cells, particularly multiple cytokine–positive CD8 T cells, indicating the induction of Ag-specific functional cytolytic T cells (Fig. 2A).

Interestingly, we found that, in addition to the direct activation of Ag-specific T cells, 1F5mG1 enhanced the overall immune responses, as illustrated by a dramatic elevation in Ki-67$^+$ (39.18 ± 7.36%), $CD44^{hi}$ (53.69 ± 3.1%), NKG2D$^+$ (10.61 ± 1.15%), and GzmB$^+$ (9.78 ± 2.75%) CD8 T cells (Fig. 2B). Similar effects of smaller magnitude were observed in CD4 T cells (data not shown). The numbers of NK cells and DCs were also increased, and their activation state was augmented, as evidenced by a higher percentage of GzmB$^+$ NK cells and $CD86^+CD40^+$ DCs (Fig. 2C, 2D). These changes were observed whether vaccine was coadministered or not. Notably, 1F5hG1 and 1F5mG2a also enhanced overall immune responses, although to a lesser extent relative to 1F5mG1 (Fig. 2B–D).

Surprisingly, despite the dramatic increase in proliferation and activation induced by 1F5mG1, an isotype that does not mediate effector cell functions (ADCC and ADCP), we observed a reduction in the frequency and total number of CD4 and CD8 T cells comparable to that induced by 1F5hG1 and 1F5mG2a (Fig. 3A). To understand the discrepancy, we further examined T cell phenotypes and their functional state after treatment with 1F5 variants. Strikingly, treatment with 1F5mG1, but not with the other isotypes, induced dramatic increases in short-lived effector cells (SLECs; defined as $CD127^-KLRG1^+CD44^{hi}CD62L^{lo}$) (52) and effector memory T cells ($T_{em}$; defined as $CD127^+KLRG1^-CD44^{hi}CD62L^{lo}$) that was accompanied by a decrease in the central memory T cells ($T_{cm}$; defined as $CD127^+KLRG1^-CD44^{hi}CD62L^{hi}$) (Fig. 3B). We also noted the upregulation and coexpression of coinhibitory molecules known to be markers of T cell exhaustion (PD-1, Lag-3, and Tim-3) and an increase in T cells that are positive for Eomes and PD-1 but lack Ki-67 expression (Fig. 3C), a truly exhausted phenotype (53). In addition, we observed elevated levels of the proapoptotic molecules Fas and aCasp3 and lower levels of the antiapoptotic molecule Bcl-2 (Fig. 3D). Similar changes in most of the parameters, albeit to a lesser extent, were observed in CD4 T cells as well (data not shown). Taken together, these assessments

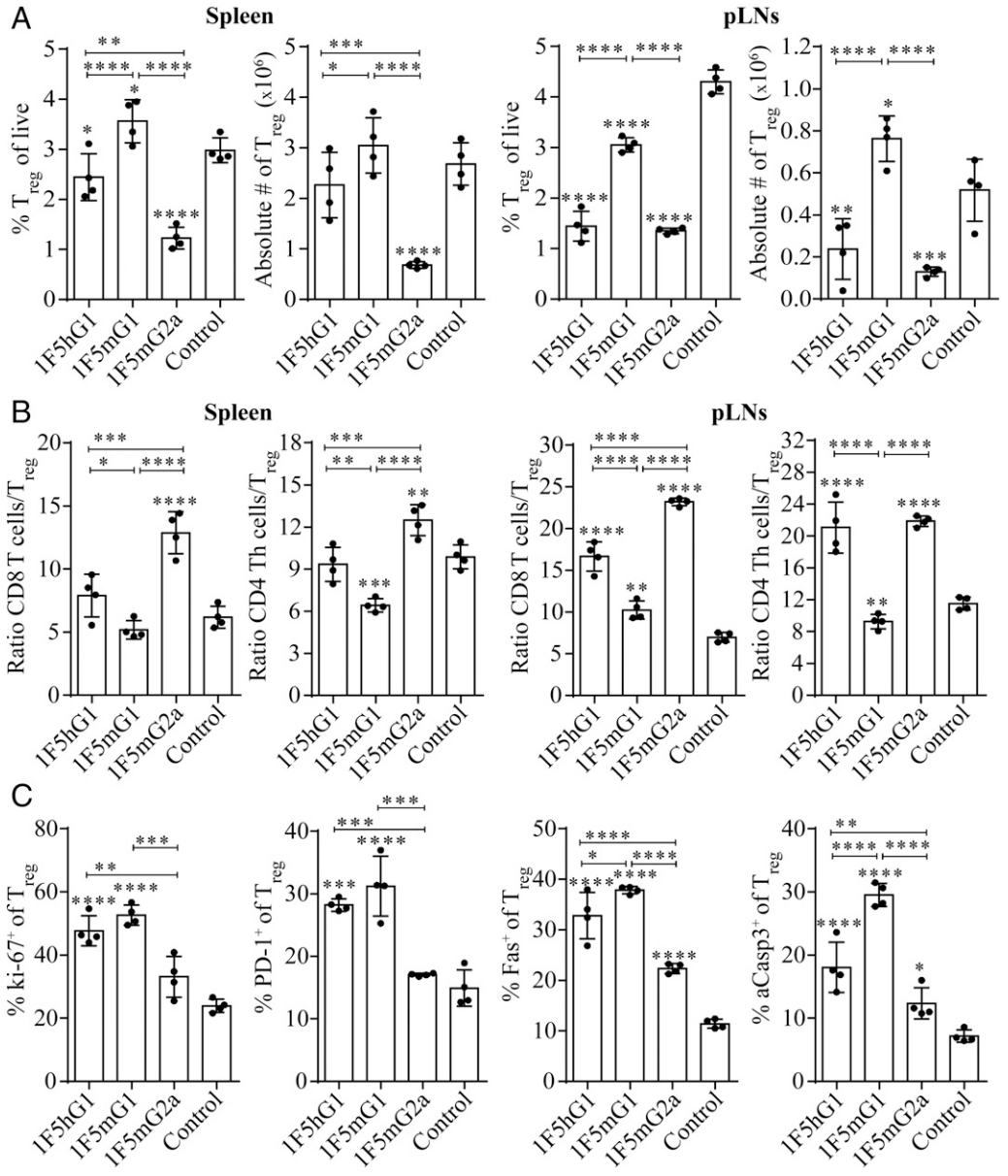


**FIGURE 4.** 1F5 variants exert differential effects on $T_{reg}$. The same preparations of splenocytes as in Fig. 3 were stained for CD4 and Foxp3 or CD25. pLNs were also collected and analyzed separately. (**A**) The percentage of $T_{reg}$ ($CD4^+Foxp3^+$) out of total live cells and their absolute numbers in spleen and pLNs. (**B**) The ratios of CD8 T cells and CD4 Th ($CD4^+Foxp3^-$) to $T_{reg}$ ($CD4^+Foxp3^+$) were calculated in spleen and pLNs. (**C**) The percentages of Ki-67, PD-1, Fas, and aCasp3 in gated $T_{reg}$ ($CD4^+CD25^+$) in the spleen. Data are representative of two independent experiments ($n$ = 3 or 4 mice per group). 2Horizontal lines indicate statistical significance between the groups specified. *$p < 0.05$, **$p < 0.01$, ***$p < 0.001$, ****$p < 0.0001$ versus control IgG.

demonstrate that strong CD27 signaling triggered by an agonistic Ab leads to CD8 and CD4 T cell proliferation, terminal differentiation, exhaustion, and apoptosis, resulting in potent, but short-lasting, immunity.

### *Targeting CD27 with depleting Ab mediates a preferential reduction in functional $T_{reg}$*

Inhibition or depletion of $T_{reg}$ has been implicated as an important mechanism of antitumor activity of immune-modulatory Abs (8–10, 54). We found that the 1F5 variants had dramatic and differential effects on $T_{reg}$. 1F5mG2a treatment resulted in a more prominent reduction in $T_{reg}$ than that observed in CD4 Th cells and CD8 T cells (Figs. 3A, 4A), which may be explained by the higher expression level of human CD27 on this subclass of T cells (Supplemental Fig. 2). The $T_{reg}$-preferential depletion led to increased ratios of CD8 T cells/$T_{reg}$ or CD4 Th cells/$T_{reg}$ in spleen and pLNs (Fig. 4B). We observed similar depleting effects with 1F5hG1, although this effect was less evident in the spleen than in the pLNs. 1F5mG1 had a marginal impact on the frequency or absolute number of $T_{reg}$. Similar to its effect on CD8 T and CD4 Th cells, 1F5mG1 increased the level of markers for proliferation, activation, and apoptosis on $T_{reg}$ (Fig. 4C).

We further tested the suppressive activity of $T_{reg}$ isolated from spleens of h*CD27*-Tg mice pretreated with the 1F5 variants (Fig. 5). $T_{reg}$ were cocultured with CFSE-labeled CD8 T cells isolated from naive mice and stimulated with CD3 Ab in vitro. $T_{reg}$ isolated from control IgG-treated mice showed potent suppression of CD8 T cell proliferation (77% inhibition) and IFN-γ production (79% inhibition). $T_{reg}$ isolated from 1F5hG1- or 1F5mG1-treated mice exhibited similar suppressive activity compared with $T_{reg}$ from control IgG-treated mice. However, $T_{reg}$ from 1F5 mG2a-treated mice weakly suppressed proliferation (34% inhibition) and

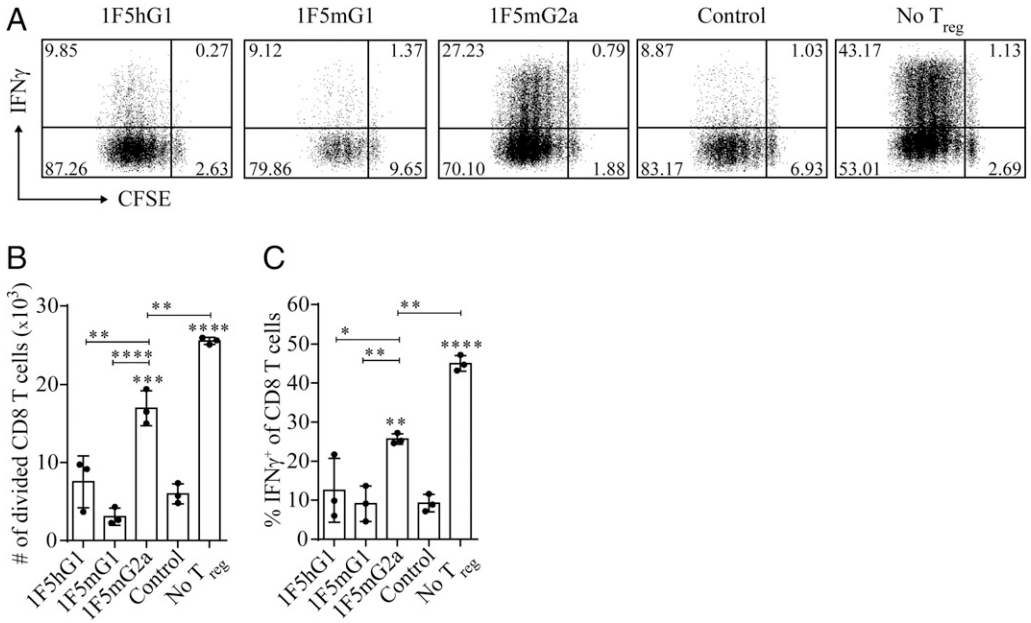


**FIGURE 5.** Residual $T_{reg}$ are less suppressive after CD27-mediated depletion. h*CD27*-Tg B6 mice were injected i.p. with 100 μg of 1F5 variants on day 0, spleens were collected on day 7, and $T_{reg}$ were isolated using CD4 and CD25 Ab-coupled beads. CD8 T cells were isolated from spleens of untreated naive mice from the same strain and labeled with CFSE. A $T_{reg}$/CD8 T cell coculture was set up at a ratio of 1:1 in CD3 Ab–coated 96-well plates in the presence of soluble CD28 Ab and incubated for 72 h. Wells containing CD8 T cells in the absence of $T_{reg}$ served as a nonsuppression reference. Cells were stained for CD4, CD8, and IFN-γ after the coculture, and all of the stained cells were acquired for flow cytometric analysis. (**A**) Representative dot plots show CFSE dilution and IFN-γ production within gated CD8 T cells from cocultures using $T_{reg}$ from the indicated treatment or a culture lacking $T_{reg}$. The numbers in each quadrant indicate the percentage of cells. (**B**) CD8 T cell proliferation was calculated based on the percentage of CD8 T cells that went through one or multiple division cycles multiplied by the total live CD8 cells acquired. (**C**) Percentage of IFN-$\gamma^+$ cells within gated CD8 T cells. Data are representative of three independent experiments ($n = 3$ mice per group). Horizontal lines indicate statistical significance between the groups specified. $^*p < 0.05$, $^{**}p < 0.01$, $^{***}p < 0.001$, $^{****}p < 0.0001$ versus control IgG.

activation (43% inhibition). We observed the same pattern of suppressive activity when we replaced CD8 T cells with CD4 Th cells (data not shown).

### *Pretreatment with depleting CD27 Ab generates long-lasting antitumor immunity*

The potent effect of 1F5mG2a on the reduction of $T_{reg}$ numbers and suppressive activity suggests that it is the dominant mechanism of antitumor activity for this isotype. To further corroborate this concept, we treated mice with a single dose of 1F5mG2a to deplete $T_{reg}$ in advance of tumor inoculation (Fig. 6A). Indeed, when 1F5mG2a was injected into h*CD27*-Tg mice 7 d prior to E.G7 tumor inoculation, very similar efficacy was observed as in the treatment given after tumor inoculation (posttreatment, Fig. 1B), with approximately half of the animals cured (referring to tumor-free survival lasting >60 d) (Fig. 6B). In the pretreatment setting, 1F5hG1 was similarly effective, despite a lower impact on $T_{reg}$ compared with 1F5mG2a. Further, 1F5mG1 pretreatment was now partially effective (20% survival), suggesting that, in addition to $T_{reg}$ depletion, the immune activation induced by 1F5 isotypes may contribute to antitumor activity. Of note, in the pretreatment setting, tumors grew before beginning to shrink, which is the same pattern observed in the posttreatment setting and is indicative of an adaptive immune response [Fig. 6C versus published data (46), and data not shown]. In fact, rechallenge of the mice that survived upon pretreatment with the 1F5 isotypes did not lead to tumor growth in any of the animals (Fig. 6D).

### *1F5mG1 and 1F5mG2a differentially impact T cells in BCL1 versus E.G7 tumor models*

We further analyzed TILs and TdLNs to understand the MOA of tumor model–dependent efficacy for the three isotypes of 1F5 Ab. BCL1 and E.G7 models were selected for the evaluation because they represented tumors being sensitive to 1F5mG1 and 1F5mG2a, respectively. In the BCL1 model, we collected spleen as the source of TILs because this is the primary site of tumor growth. Consistent with the survival data (Fig. 1A), there was remarkable reduction in spleen weights of mice treated with 1F5mG1 compared with 1F5mG2a treatment or isotype control (Fig. 7B). In the spleens of 1F5mG1-treated mice, the numbers of CD8 T cells, the ratio of CD8 T cells/$T_{reg}$, and the quality of CD8 T cells (GzmB$^+$IFN-$\gamma^+$) were significantly enhanced (Fig. 7C, 7D). However, this was also associated with an increase in the number of SLECs and a decrease in $T_{cm}$ among CD8 T cells (Fig. 7E). These observations paralleled the changes in nontumor-bearing spleens (Figs. 2, 3), suggesting that the strong agonistic effect of 1F5mG1 elicited a potent, but short-lasting, activation of CD8 T cells that led to a rapid eradication of BCL1 tumor cells in situ. In contrast, 1F5mG2a significantly reduced the number of $T_{reg}$, as well as CD8 T cells (Fig. 7C), compromising any antitumor benefit. Interestingly, 1F5hG1, which has overlapping properties of the two mouse isotypes, showed intermittent effects on TILs and antitumor activity. Collectively, the agonistic activities of the 1F5 isotypes were associated with a survival benefit in the BCL1 model.

Similar analyses of immune correlates were performed on E.G7 tumor tissue and TdLNs. Initial attempts to evaluate the TILs when animals were dosed 4 d post–tumor inoculation, and tumors were collected 7–10 d post–Ab injection, were unsuccessful because the numbers of T cells were too low for phenotypic assessment. Analysis of the TdLNs collected at the same time paralleled what was observed in the spleen and pLNs of nontumor-bearing mice (Supplemental Fig. 3 versus Figs. 2–4). We next investigated the phenotype of TILs and TdLNs using the pretreatment (day −7) model, harvesting the tumor and TdLNs at 18–20 d post–tumor

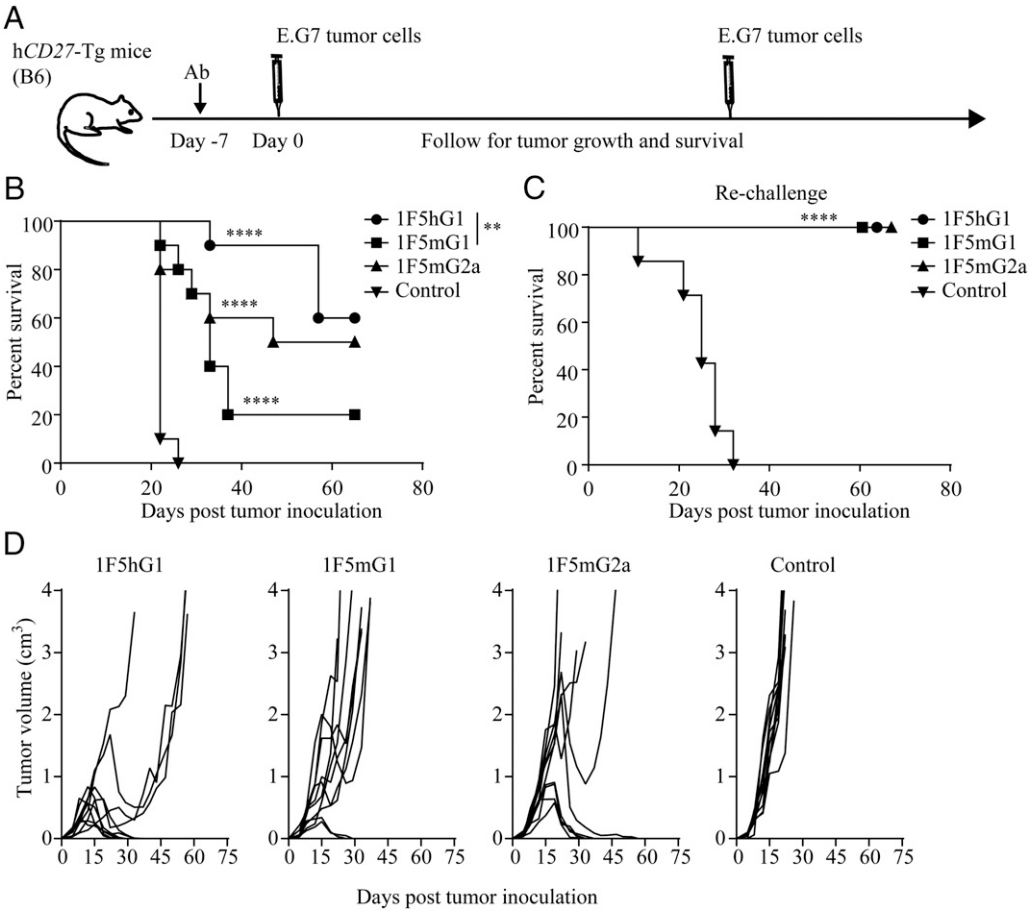


**FIGURE 6.** Pretreatment with depleting anti-CD27 Ab generates long-lasting antitumor immunity. (**A**) Treatment schema. Groups of 10 h*CD27*-Tg B6 mice were treated with 200 μg of 1F5 variants i.p. 7 d prior to inoculation with $0.5 \times 10^6$ E.G7 tumor cells s.c. on the right flank. Tumor size was measured twice a week, and mice were monitored daily for survival. Mice in which primary tumor was cured were rechallenged with $0.5 \times 10^6$ E.G7 cells s.c. on the left flank, and six naive h*CD27*-Tg B6 mice were included for tumor growth control. (**B**) Cumulative survival data from primary tumor inoculation. (**C**) Growth of the primary tumor in individual mice. (**D**) Cumulative survival data from secondary tumor inoculation. Data are representative of two independent experiments. Vertical lines indicate statistical significance between the groups specified. $^{**}p < 0.01$, $^{****}p < 0.0001$ versus control IgG.

inoculation (Fig. 8A). Such a harvest timing corresponded with initiation of tumor shrinking in 1F5mG2a- and 1F5hG1-treated mice (Fig. 6C). As expected, the tumor weights were reduced in these groups compared with the 1F5mG1 or control group (Fig. 8B). Relative to control, the percentage of TILs was increased with all 1F5 isotypes; however, the composition of the infiltrates differed. 1F5mG2a and 1F5hG1 significantly reduced $T_{reg}$ and increased CD8 T cells and NK cells, whereas 1F5mG1 increased CD4 T cells (Fig. 8B, 8C). Further, the activation of TILs, as measured by intracellular IFN-γ and GzmB without ex vivo restimulation, was greater in 1F5mG2a-treated animals relative to 1F5mG1-treated ones (Fig. 8D). Analysis of the TdLNs at this late time point showed a $T_{reg}$ reduction that was sustained to a similar extent as that observed in nontumor-bearing mice at 7 d postinjection of 1F5mG2a and 1F5hG1 (Fig. 8E versus Fig. 4A). This was accompanied by a higher percentage of $T_{cm}$ and active proliferation (Ki-67$^+$) of CD8 T cells. Finally, more activated CD8 T cells were observed in the TdLNs at baseline or responded to the ex vivo restimulation with tumor-specific SIINFEKL peptide (E.G7 is an OVA-expressing derivative of EL4 thymoma) or broad TCR stimulant CD3 Ab, as revealed by increased IFN-γ$^+$ CD8 T cells in all 1F5 variant–treated groups compared with mIgG control, with the greatest response observed in the 1F5mG2a-treated group (Fig. 8F). Collectively, all of these changes in tumor and TdLNs coincide with the differing antitumor efficacy observed with the 1F5 variants in the E.G7 model.

### *Enhanced antitumor activity results from targeting CD27 relative to CD25*

To further characterize the $T_{reg}$ reduction–dependent antitumor activity of 1F5mG2a, we compared it with the commonly used CD25-mediated $T_{reg}$ depletion with PC.61 (50, 55). We observed that pretreatment with PC.61 was not as effective as 1F5mG2a in the E.G7 tumor model (40 versus 65% cure rate and 49 d versus undefined median survival time, Fig. 9A). Increasing the dose of the PC.61 Ab did not increase the antitumor potency (data not shown). Interestingly, the combination of 1F5mG2a and PC.61 treatment enhanced the antitumor efficacy over either Ab alone (cure rate 95%, Fig. 9A). 1F5mG2a was also more effective than PC.61 in pretreatment using the CT26 tumor model (Fig. 9B).

We compared the $T_{reg}$-depletion efficiency and the suppressive activity of the residual $T_{reg}$ after using the CD27 or CD25 Ab. 1F5mG2a and PC.61 reduced $T_{reg}$ (defined as CD4$^+$Foxp3$^+$) in spleen and pLNs to a similar extent, although the number of CD4$^+$ CD25$^+$ T cells was lower with PC.61 treatment than with 1F5mG2a treatment (Fig. 9C). As may be expected, the CD27 expression level was lower on the residual $T_{reg}$ following 1F5mG2a-induced depletion; however, unexpectedly, it was significantly higher on the same cell population after CD25-mediated depletion relative to

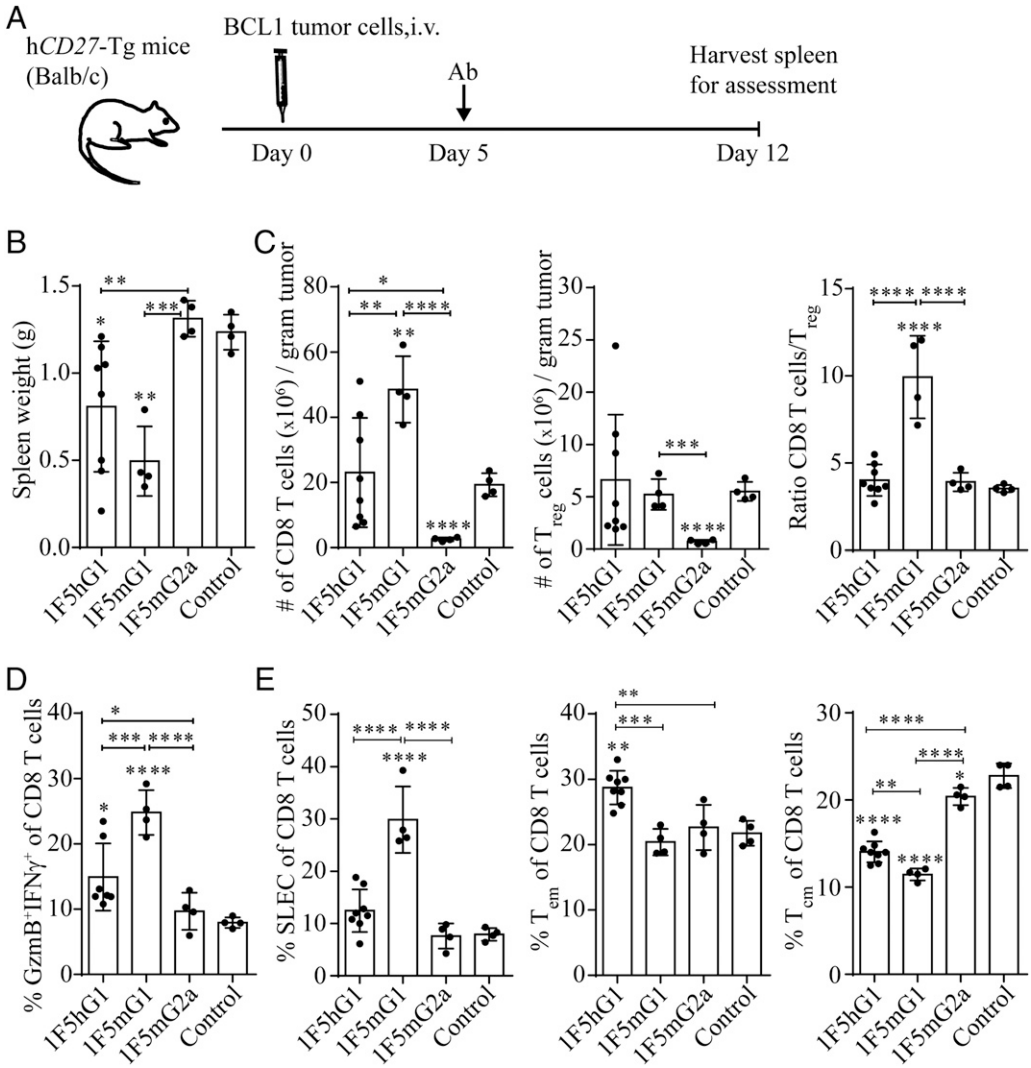


**FIGURE 7.** Changes in BCL1-bearing spleens mimic nontumor spleens upon 1F5 variants injection. (**A**) Treatment schema. h*CD27*-Tg BALB/c mice were inoculated i.v. with $3 \times 10^6$ BCL1 tumor cells on day 0 and injected i.p. with 200 μg of 1F5 variants on day 5. Spleens were collected and processed for flow cytometric analysis on day 12, as shown in the schema. (**B**) Spleen weights at harvest are depicted as bar graphs. (**C**) CD8 T cells and $T_{reg}$ ($CD4^+Foxp3^+$) are converted and depicted as the number per gram of spleen. The ratios of CD8 T cells/$T_{reg}$ were calculated. (**D**) Bulk splenocytes were stimulated ex vivo with CD3 and CD28 Abs for 5 h. Intracellular cytokines and GzmB were stained, and the percentage of IFN-γ and GzmB double-positive cells is depicted within gated CD8 T cells. (**E**) Bulk splenocytes were stained for the surface markers CD44, CD62L, and KLRG1. Percentage of SLECs ($KLRG1^+CD44^{hi}CD62L^{lo}$), $T_{em}$ ($KLRG1^-CD44^{hi}CD62L^{lo}$), and $T_{cm}$ ($KLRG1^-CD44^{hi}CD62L^{hi}$) is depicted within gated CD8 T cells. Data are representative of four independent experiments; $n = 4$ mice per group, with the exception of $n = 8$ mice in the 1F5hG1 group as a result of the large variation among mice treated with this isotype. Horizontal lines indicate statistical significance between the groups specified. $*p < 0.05$, $**p < 0.01$, $***p < 0.001$, $****p < 0.0001$ versus control IgG.

control (Fig. 9D). Interestingly, the activity of the residual $T_{reg}$ following CD25-mediated depletion was more potent in the inhibition of proliferation and IFN-γ production of activated CD8 T cells than $T_{reg}$ from mice injected with control IgG (Fig. 9E). As mentioned earlier (Fig. 5), $T_{reg}$ from mice treated with 1F5mG2a had significantly less suppressive activity. This pattern coincided with increased cytokine production among stimulated CD4 and CD8 T cells in 1F5mG2a-treated mice relative to PC.61 Ab or control (Fig. 9F).

## Discussion

In this study, we set out to understand CD27 as an immunomodulatory target and to determine the dominant mechanisms needed for an CD27 Ab to achieve antitumor efficacy. To this end, we modified the isotype of varlilumab, an Ab in clinical development, to enhance its costimulatory activity or its depleting activity, an approach that allows for the dissecting of these two MOAs. Using our human CD27–transgenic mouse model, we demonstrated that the activities of effector T cell activation and $T_{reg}$ depletion were indeed effectively modulated by altering the isotype of varlilumab, and this had a significant impact on the antitumor efficacy in various syngeneic tumor models. In general, we found that the s.c. models were more responsive to 1F5mG2a, whereas BCL1 lymphoma, which grows predominantly in the spleen, was highly responsive to 1F5mG1. Varlilumab's therapeutic effect was partial, but significant, in all models.

When comparing the agonistic activity of the varlilumab variants, we found that 1F5mG1, the only isotype that significantly engages FcγRIIB, was most effective at activating Ag-specific and nonspecific immune responses. This finding is consistent with the observation for two different agonist CD40 Abs that were shown to require FcγRIIB engagement for their agonistic and antitumor activity (48, 49). The prominent availability of FcγRIIB on splenic B cells and on BCL1 tumor cells is ideally suited for effective

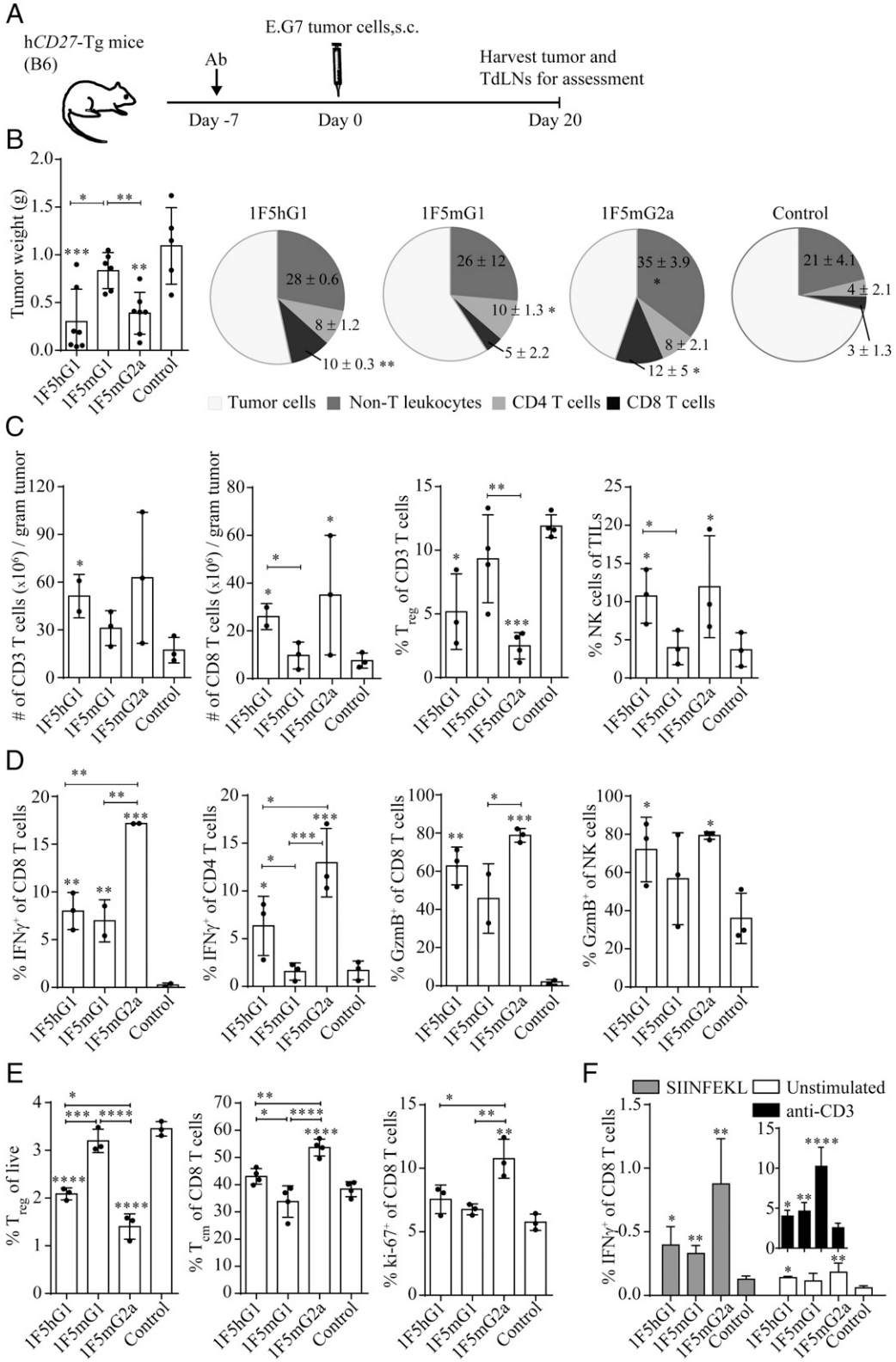


**FIGURE 8.** Delayed favorable immune correlates in the tumor and TdLNs are observed following the treatment with depleting anti-CD27 Ab. (**A**) Treatment schema. h*CD27*-Tg B6 mice were injected i.p. with 200 μg of 1F5 variants on day −7 and inoculated s.c. with $0.5 \times 10^6$ E.G7 tumor cells on day 0. Tumor and TdLNs were collected and processed for flow cytometric analysis on day 20. (**B**) Tumor weights at harvest are depicted as bar graphs. The cellular compositions of the tumors are depicted as pie graphs (tumor cells [$CD45.1^-$], CD4 T cells [$CD45.1^+CD3^+CD4^+$], CD8 T cells [$CD45.1^+CD3^+CD8^+$], and non-T leukocytes [$CD45.1^+CD3^-$]). (**C**) Total CD3 T cells and CD8 T cells per gram of tumor, percentage of $T_{reg}$ ($CD4^+Foxp3^+$) within gated CD3 T cells, and percentage of NK cells ($NK1.1^+$) within TILs. (**D**) Percentage of IFN-$\gamma^+$ cells within gated CD8 and CD4 T cells and percentage of $GzmB^+$ cells within gated CD8 T cells and within gated NK cells without ex vivo stimulation. (**E**) Percentage of $CD4^+Foxp3^+$ $T_{reg}$ out of live TdLNs cells and percentage of $KLRG1^-CD44^{hi}CD62L^{hi}$ $T_{cm}$ and Ki-$67^+$ proliferating cells within gated CD8 T cells. (**F**) TdLN cells were stimulated or not, ex vivo, with SIINFEKL peptide or with CD3 and CD28 Abs for 5 h. Intracellular IFN-γ was stained and is depicted within gated CD8 T cells. Data are representative of two independent experiments. For these experiments, eight mice per group were originally set up, and two or three (*Figure legend continues*)

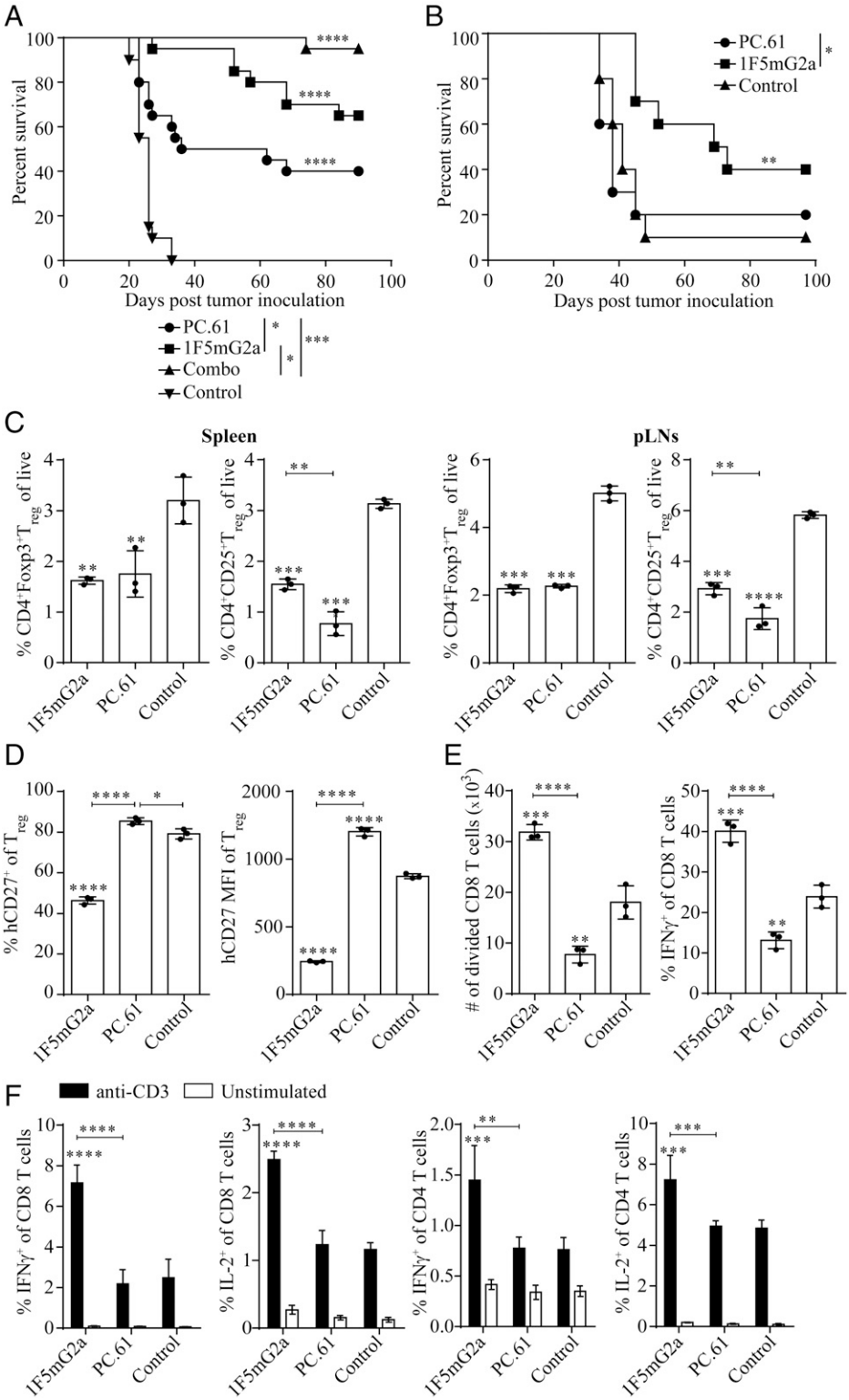


**FIGURE 9.** Targeting CD27 is superior to CD25 in reducing $T_{reg}$ suppression and antitumor efficacy. (**A**) Groups of 10 h*CD27*-Tg B6 mice were injected i.p. with 200 μg of 1F5mG2a, PC.61, 1F5mG2a and PC.61, or mIgG 7 d prior to s.c. inoculation with $0.5 \times 10^6$ E.G7 tumor cells on the right flank. Cumulative survival data are pooled from two separate studies. (**B**) Groups of 10 h*CD27*-Tg BALB/c mice were inoculated s.c. with $1 \times 10^5$ CT26 cells on day 0 and were treated with 200 μg of 1F5mG2a, PC.61, or mIgG on day 3. Cumulative survival data, representative of two separate studies, are shown. (**C**) h*CD27*-Tg B6 mice ($n = 3$ mice per group) were injected i.p. with 200 μg of 1F5mG2a, PC.61, or mIgG on day 0, and spleen and pLNs were collected on day 7. Percentage of $T_{reg}$ ($CD4^+Foxp3^+$ and $CD4^+CD25^+$) are shown. (**D**) Percentage and mean fluorescence intensity (MFI) of human CD27 on $T_{reg}$ ($CD4^+Foxp3^+$) in the spleens from (C). (**E**) $T_{reg}$ were isolated from mice treated in (C). The coculture of $T_{reg}$ and CD8 T cells was performed as described in Fig. 5. Cells were stained for CD4, CD8, and IFN-γ after the coculture, and all of the stained cells were acquired for flow cytometric analysis. CD8 T cell proliferation was calculated based on the percentage of CD8 T cells that went through one or multiple division cycles multiplied by the total live CD8 T cells acquired. (**F**) Splenocytes from mice treated in (C) were stimulated ex vivo, with or without CD3 and CD28 Abs for 5 h. Percentage of IFN-$\gamma^+$ and IL-$2^+$ cells within gated CD8 or CD4 T cells are depicted. Data are representative of two independent experiments. Horizontal or vertical lines indicate statistical significance between the groups specified. $^*p < 0.05$, $^{**}p < 0.01$, $^{***}p < 0.001$, $^{****}p < 0.0001$ versus control IgG.

cross-linking of the Ab bound to CD27 on T cells and other lymphocytes in the spleen, the primary tumor site. 1F5mG1 also led to high levels of general immune cell activation, including splenic NK cells, which can further amplify the magnitude and breadth of local immune responses, translating into effective killing of BCL1 tumor cells. Conversely, 1F5mG2a resulted in relatively weak agonist activity and reduced the number of CD8 T cells in BCL1-bearing spleen, which corresponded to no activity in this tumor model.

However, the strong agonistic activity of 1F5mG1 comes at a cost. Following the robust activation of T cells, we observed a dramatic increase in cells with a terminally differentiated phenotype and the coexpression of markers of exhaustion and apoptosis,

mice with similar tumor sizes within each group were combined at harvest for flow cytometric analysis. TdLNs were combined in a corresponding way. Horizontal lines indicate statistical significance between the groups specified. $^*p < 0.05$, $^{**}p < 0.01$, $^{***}p < 0.001$, $^{****}p < 0.0001$ versus control IgG.

indicative of AICD. This is reminiscent of T cell exhaustion and AICD that can result from continuous engagement of CD27 by its ligand, as shown in *CD70*-transgenic mice, chronic virus infection, and CD70-expressing cancers (31, 34–36, 56). Several mediators have been reported to contribute to CD27 signaling–induced T cell apoptosis, including the FasL–Fas pathway and Siva (37, 57, 58). Siva, a proapoptotic protein that binds to the intracellular cytoplasmic tail of CD27, participates in multiple apoptotic processes, including activation of caspases and mitochondrial events, and can be abrogated by the antiapoptotic protein Bcl-2 or Bcl-$x_L$ (58). The upregulation of Fas and aCasp3 and downregulation of Bcl-2 in T cells observed in this study provide evidence that multiple apoptotic pathways are activated upon potent CD27 agonism by 1F5mG1. Thus, CD27 signaling–mediated T cell apoptosis may have eliminated activated T cells, compromised memory development, and likely contributed to the generally poor efficacy of the potent agonist isotype (1F5mG1) in the s.c. tumor models.

An additional concern arises from studies reporting that CD27 signaling favors $T_{reg}$ development or survival and that the absence of CD27 in *CD27*$^{-/-}$ mice leads to slower tumor growth compared with wild-type mice (38, 39). It has also been reported that $T_{reg}$ from *CD70*$^{-/-}$ mice were reduced and not as efficient at suppressing CD4 Th cell proliferation compared with $T_{reg}$ from wild-type mice, suggesting a role for the CD70–CD27 interaction in maintaining $T_{reg}$ survival and function (59). Furthermore, surface CD70 on B cell lymphoma or leukemic cells induced Foxp3 expression in CD4 T cells or $T_{reg}$ formation (60, 61). In our study, we found that potent CD27 stimulation with the agonist 1F5mG1 led to proliferation, terminal differentiation, and apoptosis of $T_{reg}$, with little change in $T_{reg}$ number or suppressive activity.

1F5mG2a, an isotype that favors binding to activating FcγRs, was highly therapeutically effective in the s.c. tumor models. The dominant mechanism of antitumor activity for 1F5mG2a is likely from the selective depletion of suppressive $T_{reg}$. Importantly, the residual $T_{reg}$ following treatment with 1F5mG2a were found to have poor suppressive function when cocultured with in vitro–stimulated CD8 T cells or CD4 Th cells. We speculate that this reduced $T_{reg}$ activity is due to removal of the most highly suppressive $T_{reg}$ rather than a modulation of $T_{reg}$ function, in agreement with reported studies correlating the level of CD27 in $T_{reg}$ and their suppressive activity (62, 63). Additionally, 1F5mG2a does enhance Ag-specific (SIINFEKL-stimulated IFN-$\gamma^+$ CD8 T cells) and nonspecific (percentage of $CD44^+$ and percentage of Ki-$67^+$ cells among CD8 T cells, activated NK cells, and DCs) immune responses relative to control, although to a significantly lower level than 1F5mG1. We hypothesize that 1F5mG2a-mediated removal of $T_{reg}$ suppression and moderate costimulation were important in the observed antitumor efficacy and in the development of protective memory. This is supported by the superior efficacy of 1F5mG2a compared with PC.61, which only reduced $T_{reg}$ numbers.

The evaluation of immune correlates in E.G7 tumor and TdLNs at various time points also supports the hypothesis. At early time points, the numbers of tumor-infiltrated T cells were indistinguishably low in all three isotypes of 1F5-treated mice, and changes in TdLNs resemble those observed in spleen and pLNs of nontumor-bearing mice. By >3 wk after dosing of 1F5mG2a, the reduction in $T_{reg}$ was maintained, and antitumor immunity was highly elicited. Further support for the dual roles of 1F5mG2a is seen in the tumor-growth curves, which show initial growth and then gradual rejection of the tumor, independent of when the treatment was administered (day −7 or day 4 post–tumor challenge). This suggests the same MOA of 1F5mG2a in these two treatment regimens and likely involves removing $T_{reg}$ suppression and enhancing immune responses to the increasing load of tumor-specific Ags with tumor growth. Interestingly, a previous report found superior antitumor activity in the E.G7 model with a nondepleting anti-mouse CD27 Ab (RM27-3E5, rat IgG2a) compared with a depleting Ab (RM27-3C1, rat IgG2b) (43). We speculate that the lack of antitumor activity of RM27-3C1 may be due to potent and unselective reduction of T cells, including CD8 T cells, whereas the antitumor activity of RM27-3E5 may be driven by more moderate agonist properties compared with 1F5mG1.

In our studies, varlilumab (1F5hG1) generally displayed agonistic and depleting properties in between those of the 1F5mG1 and 1F5mG2a isotypes. With 1F5hG1, we could modify the level of agonism and depletion by varying the dose, such that lower doses favored agonistic activity, and higher doses led to greater depletion (Supplemental Fig. 4). We believe that the agonistic activity is a result of engaging the activating FcγRs (FcγRI and FcγRIV) at a level that is below the threshold required to trigger effector cell functions (ADCC and ADCP) but sufficient to cross-link the Ab. A similar mechanism is likely for agonist activity induced by 1F5mG2a, but a lower threshold for effector cell functions is likely required for this isotype because of its higher affinity for the activating FcγRs (FcγRI, FcγRIII, and FcγRIV). Unlike 1F5mG1, the lower agonistic activity induced by 1F5hG1 and 1F5mG2a showed no or little signs of enhancement of exhaustion and apoptosis in effector T cells. We conclude that the strongest agonistic signal is not necessarily translated to the greatest therapeutic benefit in various tumor settings and that the removal of $T_{reg}$ suppression, together with moderate costimulation, as achieved with 1F5hG1, provides effective treatment in a broader spectrum of tumor models. The animal study data with varlilumab are consistent with our early observation of varlilumab in cancer patients, which has shown evidence of T cell activation and a significant reduction in circulating $T_{reg}$ (47). However, how to best exploit these properties for effective treatment of patients will depend on a better understanding of the impact of dose and regimen on patients' immune systems.

## Acknowledgments

We thank Dr. R. Ventimiglia (Medical Communications, Celldex Therapeutics, Inc.) for critically reading and editing the manuscript.

## Disclosures

All authors are employees and shareholders of Celldex Therapeutics, Inc.

## References

1. Wolchok, J. D., H. Kluger, M. K. Callahan, M. A. Postow, N. A. Rizvi, A. M. Lesokhin, N. H. Segal, C. E. Ariyan, R. A. Gordon, K. Reed, et al. 2013. Nivolumab plus ipilimumab in advanced melanoma. *N. Engl. J. Med.* 369: 122–133.
2. Ansell, S. M., A. M. Lesokhin, I. Borrello, A. Halwani, E. C. Scott, M. Gutierrez, S. J. Schuster, M. M. Millenson, D. Cattry, G. J. Freeman, et al. 2015. PD-1 blockade with nivolumab in relapsed or refractory Hodgkin's lymphoma. *N. Engl. J. Med.* 372: 311–319.
3. Brahmer, J. R., S. S. Tykodi, L. Q. Chow, W. J. Hwu, S. L. Topalian, P. Hwu, C. G. Drake, L. H. Camacho, J. Kauh, K. Odunsi, et al. 2012. Safety and activity of anti-PD-L1 antibody in patients with advanced cancer. *N. Engl. J. Med.* 366: 2455–2465.
4. Hodi, F. S., S. J. O'Day, D. F. McDermott, R. W. Weber, J. A. Sosman, J. B. Haanen, R. Gonzalez, C. Robert, D. Schadendorf, J. C. Hassel, et al. 2010. Improved survival with ipilimumab in patients with metastatic melanoma. *N. Engl. J. Med.* 363: 711–723.
5. Topalian, S. L., F. S. Hodi, J. R. Brahmer, S. N. Gettinger, D. C. Smith, D. F. McDermott, J. D. Powderly, R. D. Carvajal, J. A. Sosman, M. B. Atkins, et al. 2012. Safety, activity, and immune correlates of anti-PD-1 antibody in cancer. *N. Engl. J. Med.* 366: 2443–2454.
6. Melero, I., D. M. Berman, M. A. Aznar, A. J. Korman, J. L. Pérez Gracia, and J. Haanen. 2015. Evolving synergistic combinations of targeted immunotherapies to combat cancer. *Nat. Rev. Cancer* 15: 457–472.

7. Mahoney, K. M., P. D. Rennert, and G. J. Freeman. 2015. Combination cancer immunotherapy and new immunomodulatory targets. *Nat. Rev. Drug Discov.* 14: 561–584.
8. Simpson, T. R., F. Li, W. Montalvo-Ortiz, M. A. Sepulveda, K. Bergerhoff, F. Arce, C. Roddie, J. Y. Henry, H. Yagita, J. D. Wolchok, et al. 2013. Fc-dependent depletion of tumor-infiltrating regulatory T cells co-defines the efficacy of anti-CTLA-4 therapy against melanoma. *J. Exp. Med.* 210: 1695–1710.
9. Bulliard, Y., R. Jolicoeur, M. Windman, S. M. Rue, S. Ettenberg, D. A. Knee, N. S. Wilson, G. Dranoff, and J. L. Brogdon. 2013. Activating Fc γ receptors contribute to the antitumor activities of immunoregulatory receptor-targeting antibodies. *J. Exp. Med.* 210: 1685–1693.
10. Bulliard, Y., R. Jolicoeur, J. Zhang, G. Dranoff, N. S. Wilson, and J. L. Brogdon. 2014. OX40 engagement depletes intratumoral Tregs via activating FcγRs, leading to antitumor efficacy. *Immunol. Cell Biol.* 92: 475–480.
11. Hintzen, R. Q., S. M. Lens, M. P. Beckmann, R. G. Goodwin, D. Lynch, and R. A. van Lier. 1994. Characterization of the human CD27 ligand, a novel member of the TNF gene family. *J. Immunol.* 152: 1762–1773.
12. Kawamura, T., Y. Ogawa, O. Shimozato, T. Ando, A. Nakao, T. Kobata, K. Okumura, H. Yagita, and S. Shimada. 2011. CD70 is selectively expressed on Th1 but not on Th2 cells and is required for Th1-type immune responses. *J. Invest. Dermatol.* 131: 1252–1261.
13. Tesselaar, K., L. A. Gravestein, G. M. van Schijndel, J. Borst, and R. A. van Lier. 1997. Characterization of murine CD70, the ligand of the TNF receptor family member CD27. *J. Immunol.* 159: 4959–4965.
14. Hintzen, R. Q., S. M. Lens, K. Lammers, H. Kuiper, M. P. Beckmann, and R. A. van Lier. 1995. Engagement of CD27 with its ligand CD70 provides a second signal for T cell activation. *J. Immunol.* 154: 2612–2623.
15. Taraban, V. Y., T. F. Rowley, D. F. Tough, and A. Al-Shamkhani. 2006. Requirement for CD70 in CD4+ Th cell-dependent and innate receptor-mediated CD8+ T cell priming. *J. Immunol.* 177: 2969–2975.
16. Keller, A. M., A. Schildknecht, Y. Xiao, M. van den Broek, and J. Borst. 2008. Expression of costimulatory ligand CD70 on steady-state dendritic cells breaks CD8+ T cell tolerance and permits effective immunity. *Immunity* 29: 934–946.
17. Keller, A. M., Y. Xiao, V. Peperzak, S. H. Naik, and J. Borst. 2009. Costimulatory ligand CD70 allows induction of CD8+ T-cell immunity by immature dendritic cells in a vaccination setting. *Blood* 113: 5167–5175.
18. Bullock, T. N., and H. Yagita. 2005. Induction of CD70 on dendritic cells through CD40 or TLR stimulation contributes to the development of CD8+ T cell responses in the absence of CD4+ T cells. *J. Immunol.* 174: 710–717.
19. Ahrends, T., N. Bąbała, Y. Xiao, H. Yagita, H. van Eenennaam, and J. Borst. 2016. CD27 agonism plus PD-1 blockade recapitulates CD4+ T-cell help in therapeutic anticancer vaccination. *Cancer Res.* 76: 2921–2931.
20. Arens, R., K. Schepers, M. A. Nolte, M. F. van Oosterwijk, R. A. van Lier, T. N. Schumacher, and M. H. van Oers. 2004. Tumor rejection induced by CD70-mediated quantitative and qualitative effects on effector CD8+ T cell formation. *J. Exp. Med.* 199: 1595–1605.
21. Dong, H., N. A. Franklin, D. J. Roberts, H. Yagita, M. J. Glennie, and T. N. Bullock. 2012. CD27 stimulation promotes the frequency of IL-7 receptor-expressing memory precursors and prevents IL-12-mediated loss of CD8(+) T cell memory in the absence of CD4(+) T cell help. *J. Immunol.* 188: 3829–3838.
22. Hendriks, J., L. A. Gravestein, K. Tesselaar, R. A. van Lier, T. N. Schumacher, and J. Borst. 2000. CD27 is required for generation and long-term maintenance of T cell immunity. *Nat. Immunol.* 1: 433–440.
23. Hendriks, J., Y. Xiao, and J. Borst. 2003. CD27 promotes survival of activated T cells and complements CD28 in generation and establishment of the effector T cell pool. *J. Exp. Med.* 198: 1369–1380.
24. Schildknecht, A., I. Miescher, H. Yagita, and M. van den Broek. 2007. Priming of CD8+ T cell responses by pathogens typically depends on CD70-mediated interactions with dendritic cells. *Eur. J. Immunol.* 37: 716–728.
25. Welten, S. P., A. Redeker, K. L. Franken, C. A. Benedict, H. Yagita, F. M. Wensveen, J. Borst, C. J. Melief, R. A. van Lier, K. P. van Gisbergen, and R. Arens. 2013. CD27-CD70 costimulation controls T cell immunity during acute and persistent cytomegalovirus infection. *J. Virol.* 87: 6851–6865.
26. Alkhairy, O. K., R. Perez-Becker, G. J. Driessen, H. Abolhassani, J. van Montfrans, S. Borte, S. Choo, N. Wang, K. Tesselaar, M. Fang, et al. 2015. Novel mutations in TNFRSF7/CD27: clinical, immunologic, and genetic characterization of human CD27 deficiency. *J. Allergy Clin. Immunol.* 136: 703–712.e710.
27. Salzer, E., S. Daschkey, S. Choo, M. Gombert, E. Santos-Valente, S. Ginzel, M. Schwendinger, O. A. Haas, G. Fritsch, W. F. Pickl, et al. 2013. Combined immunodeficiency with life-threatening EBV-associated lymphoproliferative disorder in patients lacking functional CD27. *Haematologica* 98: 473–478.
28. van Montfrans, J. M., A. I. Hoepelman, S. Otto, M. van Gijn, L. van de Corput, R. A. de Weger, L. Monaco-Shawver, P. P. Banerjee, E. A. Sanders, C. M. Jol-van der Zijde, et al. 2012. CD27 deficiency is associated with combined immunodeficiency and persistent symptomatic EBV viremia. *J. Allergy Clin. Immunol.* 129: 787–793.e6
29. Abolhassani, H., E. S. Edwards, A. Ikincioglullari, H. Jing, S. Borte, M. Buggert, L. Du, M. Matsuda-Lennikov, R. Romano, R. Caridha, et al. 2017. Combined immunodeficiency and Epstein-Barr virus–induced B cell malignancy in humans with inherited CD70 deficiency. *J. Exp. Med.* 214: 91–106.
30. Izawa, K., E. Martin, C. Soudais, J. Bruneau, D. Boutboul, R. Rodriguez, C. Lenoir, A. D. Hislop, C. Besson, F. Touzot, et al. 2017. Inherited CD70 deficiency in humans reveals a critical role for the CD70-CD27 pathway in immunity to Epstein-Barr virus infection. *J. Exp. Med.* 214: 73–89.
31. Tesselaar, K., R. Arens, G. M. van Schijndel, P. A. Baars, M. A. van der Valk, J. Borst, M. H. van Oers, and R. A. van Lier. 2003. Lethal T cell immunodeficiency induced by chronic costimulation via CD27-CD70 interactions. *Nat. Immunol.* 4: 49–54.
32. Arens, R., K. Tesselaar, P. A. Baars, G. M. van Schijndel, J. Hendriks, S. T. Pals, P. Krimpenfort, J. Borst, M. H. van Oers, and R. A. van Lier. 2001. Constitutive CD27/CD70 interaction induces expansion of effector-type T cells and results in IFNgamma-mediated B cell depletion. *Immunity* 15: 801–812.
33. De Colvenaer, V., S. Taveirne, J. Hamann, A. M. de Bruin, M. De Smedt, T. Taghon, B. Vandekerckhove, J. Plum, R. van Lier, and G. Leclercq. 2010. Continuous CD27 triggering in vivo strongly reduces NK cell numbers. *Eur. J. Immunol.* 40: 1107–1117.
34. van Gisbergen, K. P., R. W. van Olffen, J. van Beek, K. F. van der Sluijs, R. Arens, M. A. Nolte, and R. A. van Lier. 2009. Protective CD8 T cell memory is impaired during chronic CD70-driven costimulation. *J. Immunol.* 182: 5352–5362.
35. Penaloza-MacMaster, P., A. Ur Rasheed, S. S. Iyer, H. Yagita, B. R. Blazar, and R. Ahmed. 2011. Opposing effects of CD70 costimulation during acute and chronic lymphocytic choriomeningitis virus infection of mice. *J. Virol.* 85: 6168–6174.
36. Matter, M., B. Odermatt, H. Yagita, J. M. Nuoffer, and A. F. Ochsenbein. 2006. Elimination of chronic viral infection by blocking CD27 signaling. *J. Exp. Med.* 203: 2145–2155.
37. Wensveen, F. M., P. P. Unger, N. A. Kragten, I. A. Derks, A. ten Brinke, R. Arens, R. A. van Lier, E. Eldering, and K. P. van Gisbergen. 2012. CD70-driven costimulation induces survival or Fas-mediated apoptosis of T cells depending on antigenic load. *J. Immunol.* 188: 4256–4267.
38. Claus, C., C. Riether, C. Schürch, M. S. Matter, T. Hilmenyuk, and A. F. Ochsenbein. 2012. CD27 signaling increases the frequency of regulatory T cells and promotes tumor growth. *Cancer Res.* 72: 3664–3676.
39. Coquet, J. M., J. C. Ribot, N. Bąbała, S. Middendorp, G. van der Horst, Y. Xiao, J. F. Neves, D. Fonseca-Pereira, H. Jacobs, D. J. Pennington, et al. 2013. Epithelial and dendritic cells in the thymic medulla promote CD4+Foxp3+ regulatory T cell development via the CD27-CD70 pathway. *J. Exp. Med.* 210: 715–728.
40. Miller, J., G. Eisele, G. Tabatabai, S. Aulwurm, G. von Kurthy, L. Stitz, P. Roth, and M. Weller. 2010. Soluble CD70: a novel immunotherapeutic agent for experimental glioblastoma. *J. Neurosurg.* 113: 280–285.
41. Rowley, T. F., and A. Al-Shamkhani. 2004. Stimulation by soluble CD70 promotes strong primary and secondary CD8+ cytotoxic T cell responses in vivo. *J. Immunol.* 172: 6039–6046.
42. Roberts, D. J., N. A. Franklin, L. M. Kingeter, H. Yagita, A. L. Tutt, M. J. Glennie, and T. N. Bullock. 2010. Control of established melanoma by CD27 stimulation is associated with enhanced effector function and persistence, and reduced PD-1 expression of tumor infiltrating CD8(+) T cells. *J. Immunother.* 33: 769–779.
43. Sakanishi, T., and H. Yagita. 2010. Anti-tumor effects of depleting and non-depleting anti-CD27 monoclonal antibodies in immune-competent mice. *Biochem. Biophys. Res. Commun.* 393: 829–835.
44. French, R. R., V. Y. Taraban, G. R. Crowther, T. F. Rowley, J. C. Gray, P. W. Johnson, A. L. Tutt, A. Al-Shamkhani, and M. J. Glennie. 2007. Eradication of lymphoma by CD8 T cells following anti-CD40 monoclonal antibody therapy is critically dependent on CD27 costimulation. *Blood* 109: 4810–4815.
45. Vitale, L. A., L. Z. He, L. J. Thomas, J. Widger, J. Weidlick, A. Crocker, T. O'Neill, J. Storey, M. J. Glennie, D. M. Grote, et al. 2012. Development of a human monoclonal antibody for potential therapy of CD27-expressing lymphoma and leukemia. *Clin. Cancer Res.* 18: 3812–3821.
46. He, L. Z., N. Prostak, L. J. Thomas, L. Vitale, J. Weidlick, A. Crocker, C. D. Pilsmaker, S. M. Round, A. Tutt, M. J. Glennie, et al. 2013. Agonist anti-human CD27 monoclonal antibody induces T cell activation and tumor immunity in human CD27-transgenic mice. *J. Immunol.* 191: 4174–4183.
47. Burris, H. A., J. R. Infante, S. M. Ansell, J. J. Nemunaitis, G. R. Weiss, V. M. Villalobos, B. I. Sikic, M. H. Taylor, D. W. Northfelt, W. E. Carson, III., et al. 2017. Safety and activity of varlilumab, a novel and first-in-class agonist anti-CD27 antibody, in patients with advanced solid tumors. *J. Clin. Oncol.* 35: 2028–2036.
48. Li, F., and J. V. Ravetch. 2011. Inhibitory Fcγ receptor engagement drives adjuvant and anti-tumor activities of agonistic CD40 antibodies. *Science* 333: 1030–1034.
49. White, A. L., H. T. Chan, A. Roghanian, R. R. French, C. I. Mockridge, A. L. Tutt, S. V. Dixon, D. Ajona, J. S. Verbeek, A. Al-Shamkhani, et al. 2011. Interaction with FcγRIIB is critical for the agonistic activity of anti-CD40 monoclonal antibody. *J. Immunol.* 187: 1754–1763.
50. Onizuka, S., I. Tawara, J. Shimizu, S. Sakaguchi, T. Fujita, and E. Nakayama. 1999. Tumor rejection by in vivo administration of anti-CD25 (interleukin-2 receptor alpha) monoclonal antibody. *Cancer Res.* 59: 3128–3133.
51. Vonderheide, R. H., and M. J. Glennie. 2013. Agonistic CD40 antibodies and cancer therapy. *Clin. Cancer Res.* 19: 1035–1043.
52. Joshi, N. S., W. Cui, A. Chandele, H. K. Lee, D. R. Urso, J. Hagman, L. Gapin, and S. M. Kaech. 2007. Inflammation directs memory precursor and short-lived effector CD8(+) T cell fates via the graded expression of T-bet transcription factor. *Immunity* 27: 281–295.
53. Wherry, E. J., and M. Kurachi. 2015. Molecular and cellular insights into T cell exhaustion. *Nat. Rev. Immunol.* 15: 486–499.
54. Piconese, S., B. Valzasina, and M. P. Colombo. 2008. OX40 triggering blocks suppression by regulatory T cells and facilitates tumor rejection. [Published erratum appears in 2008 *J. Exp. Med.* 205: 1505.] *J. Exp. Med.* 205: 825–839.

55. Sutmuller, R. P., L. M. van Duivenvoorde, A. van Elsas, T. N. Schumacher, M. E. Wildenberg, J. P. Allison, R. E. Toes, R. Offringa, and C. J. Melief. 2001. Synergism of cytotoxic T lymphocyte-associated antigen 4 blockade and depletion of CD25(+) regulatory T cells in antitumor therapy reveals alternative pathways for suppression of autoreactive cytotoxic T lymphocyte responses. *J. Exp. Med.* 194: 823–832.
56. Diegmann, J., K. Junker, I. F. Loncarevic, S. Michel, B. Schimmel, and F. von Eggeling. 2006. Immune escape for renal cell carcinoma: CD70 mediates apoptosis in lymphocytes. *Neoplasia* 8: 933–938.
57. Arens, R., P. A. Baars, M. Jak, K. Tesselaar, M. van der Valk, M. H. van Oers, and R. A. van Lier. 2005. Cutting edge: CD95 maintains effector T cell homeostasis in chronic immune activation. *J. Immunol.* 174: 5915–5920.
58. Py, B., C. Slomianny, P. Auberger, P. X. Petit, and S. Benichou. 2004. Siva-1 and an alternative splice form lacking the death domain, Siva-2, similarly induce apoptosis in T lymphocytes via a caspase-dependent mitochondrial pathway. *J. Immunol.* 172: 4008–4017.
59. Allam, A., M. Swiecki, W. Vermi, J. D. Ashwell, and M. Colonna. 2014. Dual function of CD70 in viral infection: modulator of early cytokine responses and activator of adaptive responses. *J. Immunol.* 193: 871–878.
60. Jak, M., R. Mous, E. B. Remmerswaal, R. Spijker, A. Jaspers, A. Yagüe, E. Eldering, R. A. Van Lier, and M. H. Van Oers. 2009. Enhanced formation and survival of CD4+ CD25hi Foxp3+ T-cells in chronic lymphocytic leukemia. *Leuk. Lymphoma* 50: 788–801.
61. Yang, Z. Z., A. J. Novak, S. C. Ziesmer, T. E. Witzig, and S. M. Ansell. 2007. CD70+ non-Hodgkin lymphoma B cells induce Foxp3 expression and regulatory function in intratumoral $CD4^+CD25^-$ T cells. *Blood* 110: 2537–2544.
62. Duggleby, R. C., T. N. Shaw, L. B. Jarvis, G. Kaur, and J. S. Gaston. 2007. CD27 expression discriminates between regulatory and non-regulatory cells after expansion of human peripheral blood CD4+ CD25+ cells. *Immunology* 121: 129–139.
63. Koenen, H. J., E. Fasse, and I. Joosten. 2005. CD27/CFSE-based ex vivo selection of highly suppressive alloantigen-specific human regulatory T cells. *J. Immunol.* 174: 7573–7583.